Research Article

Development and Characterization of Colloidally Stable Dendrimer–Botox Conjugates for Targeted Muscle Delivery and Radiolabeled Imaging

Nazanin Ajdary, Maryam Davoudi, Tahereh Zadeh Mehrizi, Mehdi Shafiee Ardestani, Hasti Nequi Marnani, Hasan Ebrahimi Shahmabadi, Niloofar Ajdary

DOI: 10.34172/PS.025.42832

To appear in: Pharmaceutical Science (https://ps.tbzmed.ac.ir/)

Received date: 16 Jun 2025

Revised date: 16 Nov 2025

Accepted date: 17 Nov 2025

Please cite this article as: Ajdary N, Davoudi M, Zadeh Mehrizi T, Shafiee Ardestani M, Nequi Marnani H, Ebrahimi Shahmabadi H, et al. Development and characterization of colloidally stable dendrimer–botox conjugates for targeted muscle delivery and radiolabeled imaging. Pharm Sci. 2026. Doi: 10.34172/PS.025.42832

Development and Characterization of Colloidally Stable Dendrimer–Botox Conjugates for Targeted Muscle Delivery and Radiolabeled Imaging

Development and Characterization of Colloidally Stable Dendrimer–Botox Conjugates for Targeted Muscle Delivery and Radiolabeled Imaging

Nazanin Ajdary[1,2], Maryam Davoudi[3], Tahereh Zadeh Mehrizi[1,*], Mehdi Shafiee Ardestani[4,5,*], Hasti Nequi Marnani[1], Hasan Ebrahimi Shahmabadi[6], Niloofar Ajdary[7]

[1] *Vaccine Research Center, Iran University of Medical Sciences, Tehran, Iran*

[2] *School of Pharmacy, International Campus, Tehran University of Medical Sciences, Tehran, Iran*

[3] *Department of Medical Laboratory Sciences, School of Allied Medical Sciences, Tehran University of Medical Sciences, Tehran, Iran*

[4] *Department of Radiopharmacy, Faculty of Pharmacy, Tehran University of Medical Sciences, Tehran, Iran*

[5] *Research Center for Nuclear Medicine, Shariati Hospital, North Kargar Ave. 1411713135, Tehran, Iran*

[6] *Immunology of Infectious Diseases Research Center, Research Institute of Basic Medical Sciences, Rafsanjan University of Medical Sciences, Rafsanjan, Iran*

[7] *Student Research Committee, School of Dentistry, Alborz University of Medical Sciences, Karaj, Iran*

***Corresponding authors:**

Tahereh Zadeh Mehrizi: taherehzadehmehrizi@gmail.com; Tel: +982186703072

Mehdi Shafiee Ardestani: shafieeardestani@gmail.com; Tel: +982164122103

Running title: Radiolabeled Dendrimer–Botox for Muscle Targeting

Acknowledgements

None.

Authors' contributions

Conceptualization: Nazanin Ajdary, Tahereh Zadeh Mehrizi, Mehdi Shafiee Ardestani.

Data curation: Maryam Davoudi, Hasti Nequi Marnani.

Formal analysis: Nazanin Ajdary, Niloofar Ajdary.

Investigation: Nazanin Ajdary, Tahereh Zadeh Mehrizi, Hasti Nequi Marnani, Hasan Ebrahimi Shahmabadi, Niloofar Ajdary.

Methodology: Nazanin Ajdary, Mehdi Shafiee Ardestani, Hasti Nequi Marnani, Niloofar Ajdary.

Project administration: Mehdi Shafiee Ardestani.

Resources: Nazanin Ajdary, Mehdi Shafiee Ardestani.

Software: Maryam Davoudi, Tahereh Zadeh Mehrizi.

Supervision: Tahereh Zadeh Mehrizi, Mehdi Shafiee Ardestani.

Validation: Mehdi Shafiee Ardestani.

Visualization: Hasti Nequi Marnani.

Writing–original draft: Maryam Davoudi, Hasan Ebrahimi Shahmabadi.

Writing–review & editing: Tahereh Zadeh Mehrizi, Hasan Ebrahimi Shahmabadi.

Funding

None.

Data availability

Data are available on reasonable request. Data are available by contacting the corresponding authors on reasonable request.

Declarations

Ethics approval

Ethics approval was received from the ethics committee of Iran University of Medical Sciences (No. IR.IUMS.REC.1402.1090).

Conflict of interest

The authors declare that they have no known competing financial interests or personal relationships that could have appeared to influence the study reported in this paper.

Abstract

Background: Botox's therapeutic applications are limited by its instability and uncontrolled diffusion into extramuscular tissues. This study aims to develop a polyethylene glycol-based formulation by conjugating Botox to a second-generation anionic linear-globular dendrimer (G2-ALGDs) and evaluate its colloidal stability and muscle localization using technetium-99m radioimaging.

Methods: G2-ALGDs were synthesized via N,N'-dicyclohexylcarbodiimide catalysis and conjugated with Botox (D-BTX) using EDC/DCC coupling. Characterization was done by DLS, FTIR, AFM, TEM, and FE-SEM. Stability at 4 °C was monitored for six months using DLS and TEM. Cytocompatibility was assessed by MTT assay in HFF2 cells. D-BTX was radiolabeled with technetium-99m to study purity, stability, and *in vivo* biodistribution using RT-LC and SPECT imaging.

Results: Botox conjugation increased the particle size from 111.6 ± 16.9 nm to 160.0 ± 3.1 nm and shifted the zeta potential from –25.2 ± 1.63 mV to +17.16 ± 1.24 mV. FTIR confirmed amide bond formation at 1649 cm^{-1}. D-BTX was much less cytotoxic than free Botox at 0.001 ng/mL ($p = 0.0013$), but no difference was observed at higher concentrations. The formulation exhibited physical stability for six months at 4°C. The radiolabeled formulation was up to 90.85% pure and remained stable for 24 h. SPECT imaging revealed improved localization of D-BTX within the muscle. After 12 h, D-BTX exhibited maximum signal intensity with minimal dispersion, indicative of controlled diffusion at the injection site.

Conclusion: This PEGylated dendrimer-Botox nanoconjugate provides a stable, muscle-targeting, and imageable platform, which surmounts some of the main drawbacks in current clinical applications.

Keywords: Botox; Stability; Technetium 99m; ALGD; Single photon emission computed tomography

Graphical Abstract

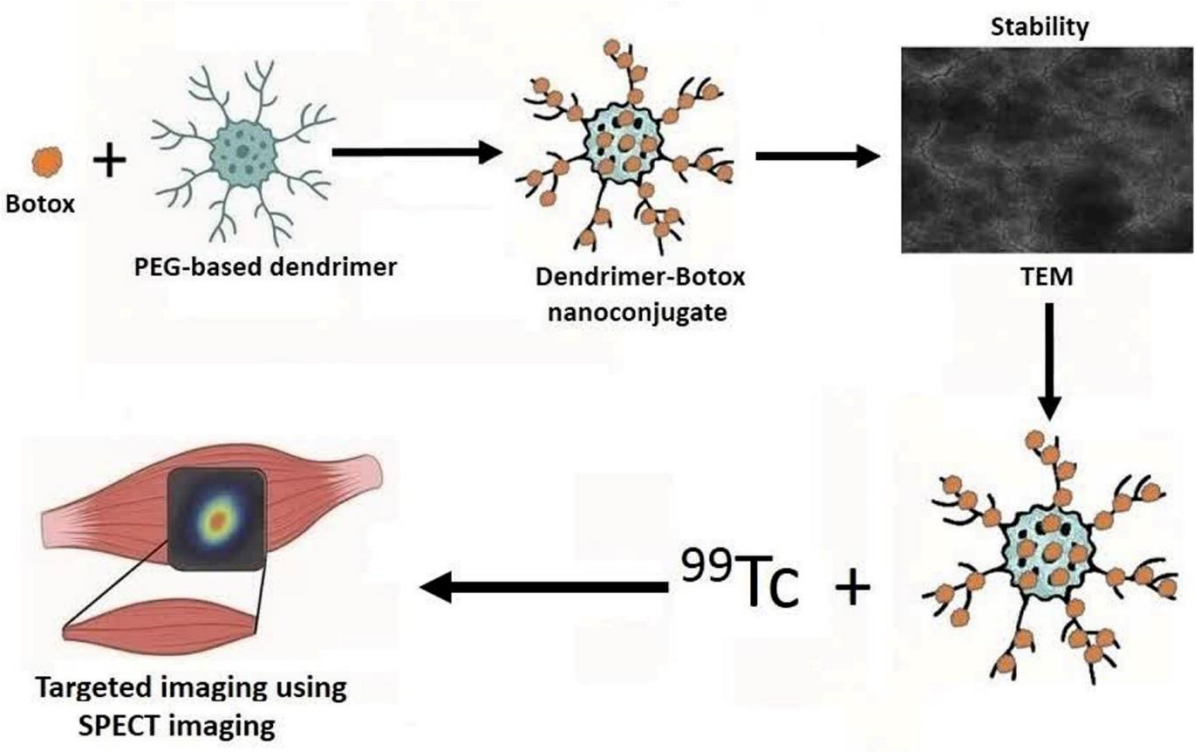

Introduction

Botulinum neurotoxin (BTX), the highly potent exotoxin of *Clostridium botulinum*, inhibits acetylcholine release at neuromuscular junctions.[1-3] BTX has been an outstanding therapeutic drug in certain neuromuscular disease conditions, e.g., spasticity and dystonia, as well as dermatological/cosmetic applications for treatment of wrinkles and hyperhidrosis.[4-6] This toxin is available in a variety of serotypes (A–G) that differ in their substrate specificity and pharmacological behavior.[7-10] BTX-A, the most clinically applicable serotype, cleaves Synaptosomal-associated protein 25 (SNAP-25) to trigger its neuromodulatory effect. This serotype is clinically approved in a variety of different preparations, e.g., BOTOX®.[11, 12]

Structurally, BTX is a 150 kDa protein that complexes with non-toxic accessory proteins to form larger toxin complexes. The BTX-A complex, for example, can be present in 900 kDa, 500 kDa, and 360 kDa forms.[13, 14] These neurotoxin complexes contain non-toxic hemagglutinin (HA) and non-toxic non-hemagglutinin (NTNH) proteins, which are believed to enhance toxin stability, withstand enzymatic degradation, and control rates of diffusion upon intramuscular injection.[3, 10, 15] Larger toxin complexes may also influence the pharmacokinetics of BTX by changing its rate of diffusion from the injection site, thereby influencing both therapeutic efficacy and safety.[10, 16]

Various commercial Botox products are used globally (Table 1), all of which contain varying primary attributes such as the manufacturing process, excipient matrix, molecular weight range, storage conditions, and post-reconstitution stability.[17-22] All these differences play a vital role in affecting their clinical effect, immunogenicity, and product stability to a large extent. Despite widespread use for therapeutic and cosmetic treatment, concerns regarding cold chain dependency and limited shelf-life remain prominent.[10, 17-29] One of the major challenges in

formulating BTX is its degradation at several stages of the process, from bacterial culture and fermentation to purification and drug formulation.[8, 30] Interestingly, the conversion of milligram quantities in bacterial culture to nanogram per milliliter doses in injectable form makes this toxin highly unstable.[31] As a result, Botox is usually prepared as a freeze-dried lyophilized powder that requires reconstitution with saline for injection.[30, 32] However, this agent is quite unstable after reconstitution and rapidly loses its biological activity.[26] This liability is exacerbated by conditions such as temperature fluctuations, surface denaturation, and exposure to high pH levels that can lead to degradation or production of inactive toxoid proteins.[26-28] Thus, the development of new formulations to stabilize and enhance the specificity of action of Botox holds a value of utmost importance to obviate such limitations and optimize its clinical potency.

There are other restrictions on the use of Botox in clinical settings. The beneficial effects of this agent, e.g., to soften wrinkles or relieve spasms of muscle, usually persist for three months, and injections have to be repeated to continue to achieve these effects over time.[33, 34] This is a significant burden for patients who receive repeated injections and contributes to the risk of side effects such as pain, hematoma, bruising, and, infrequently, accidental paralysis of muscles or eyelid ptosis secondary to toxin release.[35, 36] While many cooling techniques and other treatments have been investigated to minimize discomfort, the invasiveness of Botox injections remains a disadvantage.[37] Moreover, frequent injections induce an immune response by triggering antibodies and decreasing therapeutic effects over time.[38-40] Efforts should be undertaken to develop long-acting and stable drugs to lower the rate of painful injections.[41]

Nanotechnology-delivery systems have shown considerable promise in improving the pharmacological profile of peptide drugs such as Botox.[42-48] The nanoformulations yield higher

protection of the bioactive drug, sustained release profiles, reduced dosing frequencies, and targeted delivery with low systemic exposure.[10, 27, 49-65] Among numerous nanocarriers, dendrimers, namely anionic linear-globular dendrimers (ALGDs) synthesized from biocompatible monomers like citric acid and polyethylene glycol (PEG), are exceptional in that they have a monodisperse architecture, tunable surface chemistry, and stable conjugation capacity of proteins and peptides via ester or amide bonds.[48, 66-71]

The biological activity of nano-Botox can be assessed using several well-known methods that assess its enzymatic activity or functional effects *in vivo*. At the molecular level, the SNAP-25 endopeptidase assay based on fluorescence resonance energy transfer (FRET) has been applied to quantify the specific cleavage activity of the toxin on its intracellular substrate.[10, 49] For functional validation, the *in vivo* lethal dose (LD_{50}) and paralysis assays in mouse models remain the classic criteria for determining the functional potency and durability.[10, 49, 52] In addition, the Aoki scale scoring system has been developed to provide a semiquantitative assessment of muscle paralysis after nano-Botox administration in animal models.[10] Furthermore, the therapeutic significance of Botox formulations can be confirmed in clinical settings, where tests such as Maximal Brow Elevation and wrinkle severity scoring can be used to assess the toxin retention and durability.[10, 72]

To enable *in vivo* tracking of nanoformulated Botox, its radiolabeling with technetium-99m (^{99m}Tc) offers a non-invasive and extremely sensitive approach. Compared to iodine-based radiolabels, ^{99m}Tc possesses favorable imaging qualities with minimal effect on biological function, and it is therefore the agent of choice for preclinical biodistribution studies and clinical diagnostic imaging.[73, 74] Therefore, this study aimed to nanosize Botox with dendritic

nanoparticles to improve its colloidal stability and evaluate its potential for targeted muscle delivery and radiolabel imaging. By incorporating Botox into a dendrimeric matrix, we are attempting to develop a less toxic, more stable, muscle-targeted, and longer-lasting therapeutic preparation that enhances the safety, convenience, and overall efficacy of botulinum toxin-based therapy.

Materials and Methods

Materials

The following materials were utilized in this study: Dicarboxylated polyethylene glycol 600 Da (PEG-600; Merck, Germany), Botox (MASPORT®500; MasoonDarou, Iran), N, N'-dicyclohexylcarbodiimide (DCC; Sigma-Aldrich, USA), dimethylformamide (DMF; Chemex, China), citric acid (Kimia Tehran Acid Company, Iran), ^{99}Mo/^{99m}Tc generator (Pars Isotope, Iran), 1-ethyl-3-(3-dimethylaminopropyl) carbodiimide hydrochloride (EDC; Sigma-Aldrich, USA), high-glucose Dulbecco's Modified Eagle Medium (DMEM; Merck, Germany), fetal bovine serum (FBS; Merck, Germany), and dimethyl sulfoxide (DMSO; Sigma-Aldrich, USA). Sephadex G-series gel filtration media was obtained from Sigma-Aldrich. Human foreskin fibroblast 2 (HFF2) cell lines were used for *in vitro* cytotoxicity assays. Male BALB/c mice (age: 6 months; body weight: approximately 35 g) were employed for *in vivo* biodistribution studies.

Synthesis and purification of ALGD dendrimers

G2-ALGD dendrimers were synthesized via the divergent approach and purified later by gel filtration chromatography. Briefly, 2 mL of PEG-600 was initially mixed with 5 mL of DMF in a dry

Erlenmeyer flask. To the solution, 0.2 g of calcium chloride was added to initiate dehydration of the medium, and then the solution was stirred at room temperature for 15 min. Subsequently, 0.15 g of DCC and 0.15 g of citric acid were added to the reaction mixture and stirred for 1 h. An additional 0.15 g of DCC and 0.15 g of citric acid were added, and the reaction was allowed to proceed under constant stirring for 8 days at room temperature for dendrimer polymerization. Upon completion of the reaction, 5 mL of distilled water was introduced to the reaction content, and the aqueous solution was filtered to remove insoluble impurities. Filtrate was then cleaned up using a Sephadex column to clean the dendrimer product. The cleaned-up solution was subsequently concentrated in a rotary evaporator to remove excess water. The synthesized dendrimer was finally lyophilized and stored at −20 °C for three days before the conjugation and characterization steps.

Characterization of the synthesized nanodendrimers

Dynamic light scattering (DLS)

Hydrodynamic diameter, polydispersity index (PDI), and zeta potential of the prepared dendrimers were obtained by employing a Zetasizer SZ100 (Horiba, Japan). Dendrimer suspensions were appropriately diluted with deionized water, and their absorbance was obtained at 630 nm. The measurements were performed at 25 °C, and the data were obtained by averaging three independent experiments.

Fourier transform infrared spectroscopy (FTIR)

For analysis of the chemical structure and functional group content of dendrimers, FTIR analysis was performed on an Avatar FTIR spectrophotometer (Thermo Scientific, USA). A small quantity of lyophilized samples was ground to a fine powder and mixed with potassium bromide (KBr) in a 5:95 (w/w) proportion. The solution was hydraulically compressed into a clear pellet and mid-infrared scanned for characteristic amide and ester bond absorption peaks to determine dendrimer formation and potential sites of conjugation.

Atomic force microscopy (AFM)

G2-ALGD dendrimers' surface morphology and nanoscale surface topography were imaged by atomic force microscopy (JPK NanoWizard II, Bruker, Germany). Dendrimers were dissolved in an aqueous solution of double-distilled water at a concentration of 100 µM. An aliquot drop was deposited on a freshly cleaned glass slide and allowed to dry in a vacuum using a desiccator. Finally, 2D and 3D images were recorded in non-contact mode, and data were analyzed with JPK Data Processing Software version 7.0 to evaluate particle shape, distribution, and surface properties.

Transmission electron microscopy (TEM)

Dendrimers were suspended in deionized water to a concentration level of 1 mg/mL. For uniformity of samples, the suspension was sonicated for 5 min. Substrates were copper TEM grids coated with a carbon support film. To ensure better adhesion of the samples, the grids were rendered hydrophilic using glow discharge treatment prior to the deposition of the sample. An aliquot of the suspension equivalent to 5 µL was dropped slowly onto the surface of the treated

grid and left for 1–2 min. Trapped liquid was removed by running a piece of filter paper very lightly against the edge of the grid. The grids were left for a minimum period of 30 min to dry in the room at ambient temperatures. Where necessary, to provide contrast, negative staining was obtained with a 2% (w/v) solution of aqueous phosphotungstic acid (PTA). TEM images were captured on a Philips CM120 transmission electron microscope (Philips, Netherlands) operated at an accelerating voltage of 100 kV. Regions of interest were selected and captured at appropriate magnifications. Image analysis of particle morphology was done using ImageJ software (National Institutes of Health, USA).

Field emission scanning electron microscopy (FE-SEM)

For the study of surface topography, FE-SEM analysis was conducted on TESCAN instruments (models: VEGA3, MIRA II, and MIRA III; Czech Republic). Sample preparation was carried out by the drop-casting method, a widely used technique for immobilizing suspensions of nanoparticles on conductive surfaces. Suspension of dendrimers was prepared in deionized water at a concentration of 1 mg/mL. To avoid nanoparticle agglomeration, the suspension was sonicated for 10 min. A 10–50 µL aliquot was then gently deposited on a conductive carbon adhesive strip mounted on an aluminum stub using a micropipette. The samples were left to air dry at room temperature for 2 to 4 h to allow complete evaporation of the solvent, leaving behind only the nanoparticles that had become adhered to the surface without modifying their original structure. Once dried completely, the sample surface was sputter-coated with a thin gold conductive film (~5–10 nm) using a sputter coater.

G2-ALGD dendrimer conjugation with Botox

For the formation of the dendrimer-Botox (D-BTX) complex, DMF (10 mL), MASPORT®500 (2 mL), and the G2-ALGD dendrimers (2 mL) were taken in solution and gently stirred for 15 min. Then, EDC (0.2 mg) and DCC (2 mL) were added to the reaction mixture to form an amide bond between the carboxyl groups of the dendrimers and the amine groups of BTX-A. The solution was kept at room temperature under stirring for 7 days to ensure complete conjugation. At the end of this process, the resulting G2-BTX nanocomposites were characterized by physicochemical characterization methods such as DLS, FTIR, AFM, TEM, and FE-SEM, as discussed in Section 2.3.

In vitro studies

Stability assessment

Colloidal stability of the D-BTX formulation was evaluated at 3 and 6 months. The formulations were stored at 4 °C and protected from light in sealed vials. Hydrodynamic diameter and zeta potential were confirmed by DLS, and morphological stability was confirmed by TEM imaging. Triplicate samples were assessed at each time point and then compared with their baseline values to determine whether aggregation, degradation, or disruption of the integrity of the nanoparticles occurred during the storage process.

Cytotoxicity evaluation

Cytotoxic impacts of free Botox, G2-ALGD dendrimers, and D-BTX were evaluated against HFF2 using the MTT assay, which measures the mitochondrial metabolic activity as an indicator of cell viability. HFF2 cells were cultured at a density of 2×10^4 cells/well in a 96-well plate containing

200 µl of DMEM medium supplemented with 10% FBS. After 24 h of incubation in normal culture conditions (37 °C, 5% CO_2), different concentrations (0.001, 0.01, and 0.1 ng/mL) of free Botox, G2-ALGD dendrimers, and D-BTX were added to the cells and incubated again for another 24 h. On the second day, the wells were given 20 µL of the MTT solution (5 mg/mL in PBS). The plates were incubated for 4 h in the dark at 37 °C, after which the culture medium was pipetted out of each well and 100 µL of DMSO was added to the wells to dissolve the formazan crystals. The plates were shaken at 100 rpm for 10 min at 37 °C. Absorbance at 570 nm was read using a microplate reader (Agilent BioTek, USA). Cell viability was estimated by using the following equation:

$$Viability\ (\%) = \frac{\text{Absorbance of treated cells}}{\text{Absorbance of control cells}} \times 100$$

Intracorporeal tracking guided by the radiotracer Tc^{99m}

Preparation of the Tin(II) chloride reducing agent

To reduce pertechnetate ions ($^{99m}TcO_4^-$), a freshly prepared solution of stannous chloride ($SnCl_2{\cdot}2H_2O$) was used. For this, 1 mg of $SnCl_2{\cdot}2H_2O$ powder was accurately weighed and dissolved in 1 mL of 0.1 M hydrochloric acid (HCl). The preparation was carried out under air-free conditions to prevent oxidation and was used immediately after preparation.

^{99m}Tc-Radiolabeling procedure of the dendrimer–botox complex

Optimal radiolabeling conditions—including $SnCl_2$ concentration, ligand-to-metal ratio, pH, temperature, and incubation time—were initially optimized. The optimal protocol was as follows: 3 mCi of the dose-calibrated ^{99m}Tc-pertechnetate solution was pipetted into a reaction vial. Next,

25 µL of the newly made $SnCl_2$ reducing agent was added to the vial, and the vial was incubated at room temperature for 15 min to allow technetium reduction. To complete labeling, 50 µL of the D–BTX conjugate was added to the reaction vial, and the mixture was allowed to sit at room temperature for half an hour. Mechanism-wise, $SnCl_2$ reduces pertechnetate ($^{99m}TcO_4^-$) to a lower oxidation state, allowing coordination with the abundant surface oxygen donor groups (–OH and –COOH) present in the G2-ALGD dendrimers. These oxygen atoms donate non-bonding electron pairs to technetium, which leads to the formation of a stable dendrimer-technetium complex. This process is mechanistically similar to the chelation observed with polyaminocarboxylate ligands such as DTPA.

Radiochemical purity assessment

Radiochemical purity of the ^{99m}Tc-labeled D–BTX complex was evaluated by radio-thin layer chromatography (RT-LC). The RT-LC analysis was performed with the help of the RTLC2118 system (Shinjin Medics, South Korea). Approximately 5 µL of the radiolabeled complex was spotted on the baseline of a silica gel-coated strip of chromatography. The strip was set up in a chromatographic chamber with acetone used as the mobile phase. When the solvent front had traveled a distance of approximately 10 cm, the strip was removed and air-dried. The RTLC2118 gamma detector then scanned the dried strip. In this system, free $^{99m}TcO_4^-$ migrated with the solvent front and displayed a retention factor (Rf) close to 1. In contrast, the radiolabeled D–BTX complex and colloidal $^{99m}TcO_2$ remained at the origin, showing an Rf close to 0. The device quantified the activity of free pertechnetate and colloidal technetium. We first performed independent quality control on freshly washed technetium (^{99m}Tc) from the generator using

radiochemical purity testing methods. The results consistently showed that the colloidal impurity content ($^{99m}TcO_2$) was less than 2%. Therefore, in our labeling experiments, when both D-BTX-^{99m}Tc and $^{99m}TcO_2$ were present in the same Rf region, we attributed up to 2% of the total activity to $^{99m}TcO_2$, with the remainder being due to the labeled dendrimer-Botox complex. The radiochemical purity was calculated using the following formula:[75, 76]

Radiochemical Purity (%)=100−(%$^{99m}TcO_4^-$+%$^{99m}TcO_2$)

Radiochemical stability testing

To determine the relative radiochemical stability of D-BTX nanoconjugates and dendrimates, all the samples were tagged with approximately 0.5 mCi of ^{99m}Tc and dispersed in PBS (pH ~7.0) to simulate physiological conditions. Samples were stored at 37 °C in a jacketed water bath incubator. Aliquots were tested at predetermined time intervals: 0, 1, 2, 4, 6, 8, 12, and 24 h. Radiochemical stability was measured using the RT-LC method. After drying, radioactivity along each strip was measured quantitatively using a gamma counter. The percentage of free pertechnetate compared to the overall radioactivity was calculated. Every measurement was taken in triplicate, and values were reported in the form of mean ± SD. It was defined as radiochemically stable when at any observed point of time, the free pertechnetate percentage never exceeded the value of 10%.

Imaging Study of the ^{99m}Tc-labeled formulations

Ethics approval was received from the ethics committee of Iran University of Medical Sciences (No. IR.IUMS.REC.1402.1090). Six-month-old male BALB/c mice (weight: ~35 g) were randomly

assigned to one of the following groups (n = 3 per group): (i) D-BTX-^{99m}Tc group: Treated with radiolabeled dendrimer-Botox conjugates; (ii) Free ^{99m}Tc control group: Treated with unbound ^{99m}Tc-pertechnetate; (iii) D-^{99m}Tc group: Treated with dendrimer conjugated with ^{99m}Tc; and (IV) Botox-^{99m}Tc group: Treated with radiolabeled botulinum toxin without dendrimer. The animal of every group received an intramuscular injection of 0.5 mCi of the respective radiolabeled formulation into the hind limb muscle following light anesthesia caused by ketamine–xylazine (KX). Mice were imaged under anesthesia by intraperitoneal (IP) injection of ketamine (80 mg/kg) and xylazine (10 mg/kg). Whole-body SPECT imaging was performed using the HiReSPECT imaging system immediately after injection and again at one hour post-injection. The intrinsic gamma counters of the whole-body SPECT system allowed real-time measurement of gamma radiation from ^{99m}Tc. The non-invasive imaging method provided information on the *in vivo* kinetic properties and stability of the radiopharmaceutical.

Quantitative analysis of the SPECT images was done with ImageJ software (National Institutes of Health, USA). Regions of interest (ROIs) were traced manually over the injection site to measure the area of technetium-99m signal dispersion in muscle tissue. Area (pixel^2), Mean intensity, Minimum (Min), and Maximum (Max) intensity values were recorded for each sample at varying time points for comparing retention and diffusion behavior of all formulations within the muscles.

Statistical analysis

All measurements were reported as mean ± standard deviation (SD). Normality of data distribution was tested using the Shapiro–Wilk test. Comparisons of the groups were made using

one-way analysis of variance (ANOVA) and Tukey's post hoc multiple comparison test. Statistical analysis was conducted on SPSS software (version 24.0; IBM Corp., Armonk, NY, USA). GraphPad Prism (GraphPad Software Inc., USA) was employed for plotting graphs. A p-value of < 0.05 was considered to indicate statistical significance.

Results

DLS characterization

Zeta potential and hydrodynamic diameter of the unloaded G2 dendrimers and D-BTX were determined by DLS. Results are shown in Table 2. The particle size of G2 dendrimers was 111.6 ± 16.9 nm, while that of the D-BTX conjugates was 160.0 ± 3.1 nm, which confirms successful Botox conjugation. The PDI of the samples was low, with narrow and unimodal peaks in the DLS profiles (Figure 1A and C), which suggested homogeneous populations of nanoparticles. The surface charge was measured by zeta potential analysis and established the –25.2 ± 1.63 mV surface charge of the unloaded G2 dendrimers, as would be expected for the terminal carboxyl groups. The zeta potential of resulting D-BTX conjugates reversed to +17.16 ± 1.24 mV after conjugation (Figure 1B and D). This drastic change in surface charge again reflects the formation of a stable conjugate through electrostatic and covalent bonds.

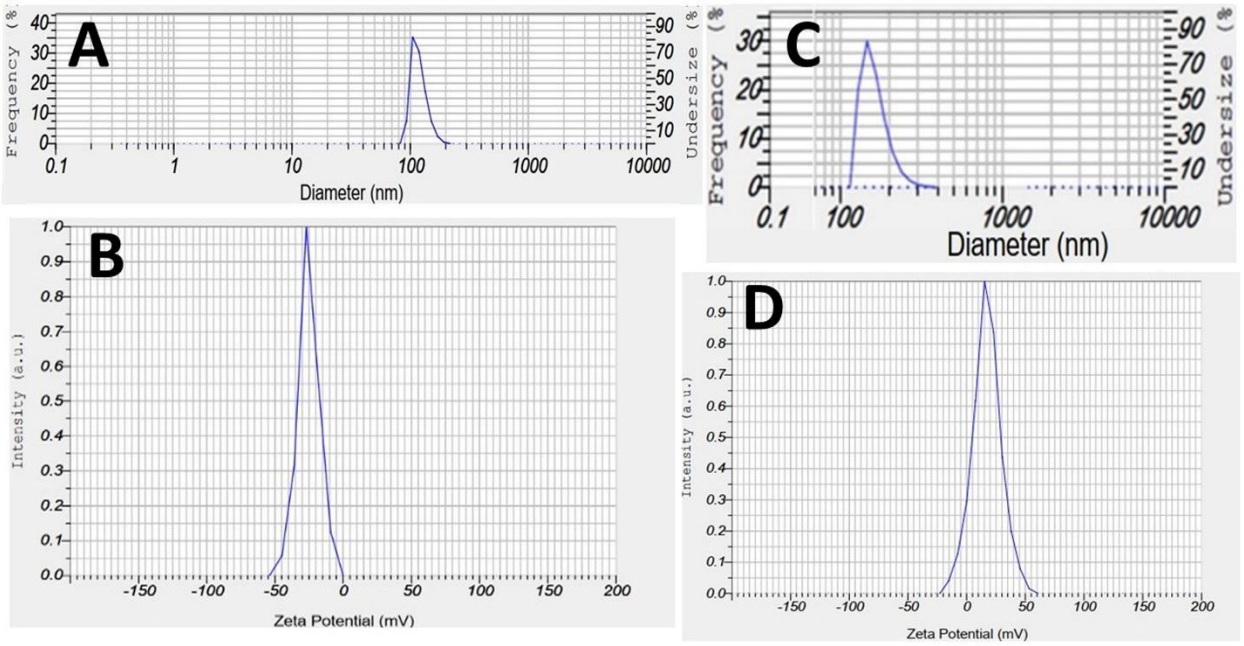

Figure 1. DLS analysis of free dendrimers and D-BTX nanoconjugates. (**A**) Particle size distribution of G2 dendrimers; (**B**) Zeta potential of G2 dendrimers; (**C**) Particle size distribution of D-BTX conjugates; (**D**) Zeta potential of D-BTX conjugates.

FTIR spectroscopic analysis

Table 3 tabulates the major absorption bands for all preparations, and Figure 2 shows the FTIR spectra for G2 dendrimer and D-BTX conjugates, respectively. In the process of G2 dendrimer, there were some varying peaks at 1232.9 cm^{-1} (the C-O stretching of the ester bonds) and 1726 cm^{-1} (the C=O ester bonds of citric acid), indicating successful dendrimer synthesis. Upon complexation with Botox, a very intense peak at 1649 cm^{-1} was observed corresponding to amide I vibrations (C=O stretching). Most likely, an amide bond of such type was formed between the amine groups of BTX-A and the carboxyl groups of the dendrimer. The presence of such a peak indicated that the chemical conjugation reaction had succeeded.

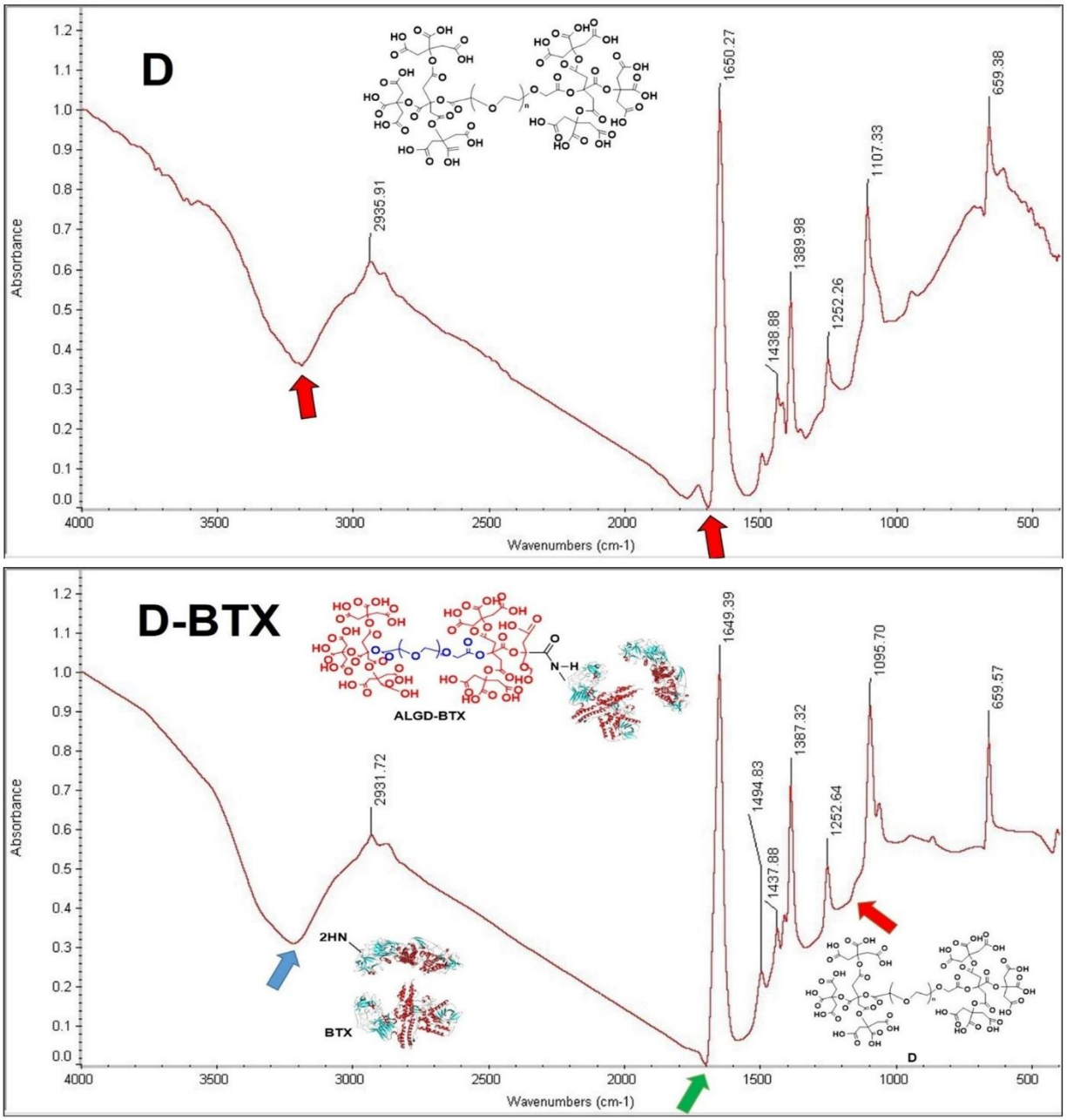

Figure 2. FTIR spectra of G2 dendrimer (D) and G2 dendrimer-BTX conjugate (D-BTX). The characteristic bands corresponding to ester and amide groups are indicated.

AFM analysis

This experiment was utilized to examine the nanostructure and surface morphology of the unloaded D-BTX and G2 dendrimers. Figure 3 illustrates the 2D and 3D topographs. The G2 dendrimers displayed a fairly uniform, needle-like morphology of nanoscale size, while the D-BTX conjugates had broad, hill-like surface features typical of drug loading. The morphological shift from the thin, sharp features in the unloaded dendrimers to rounder, taller features in the conjugated nanoparticles supported the attachment of the Botox onto the surface of the dendrimer.

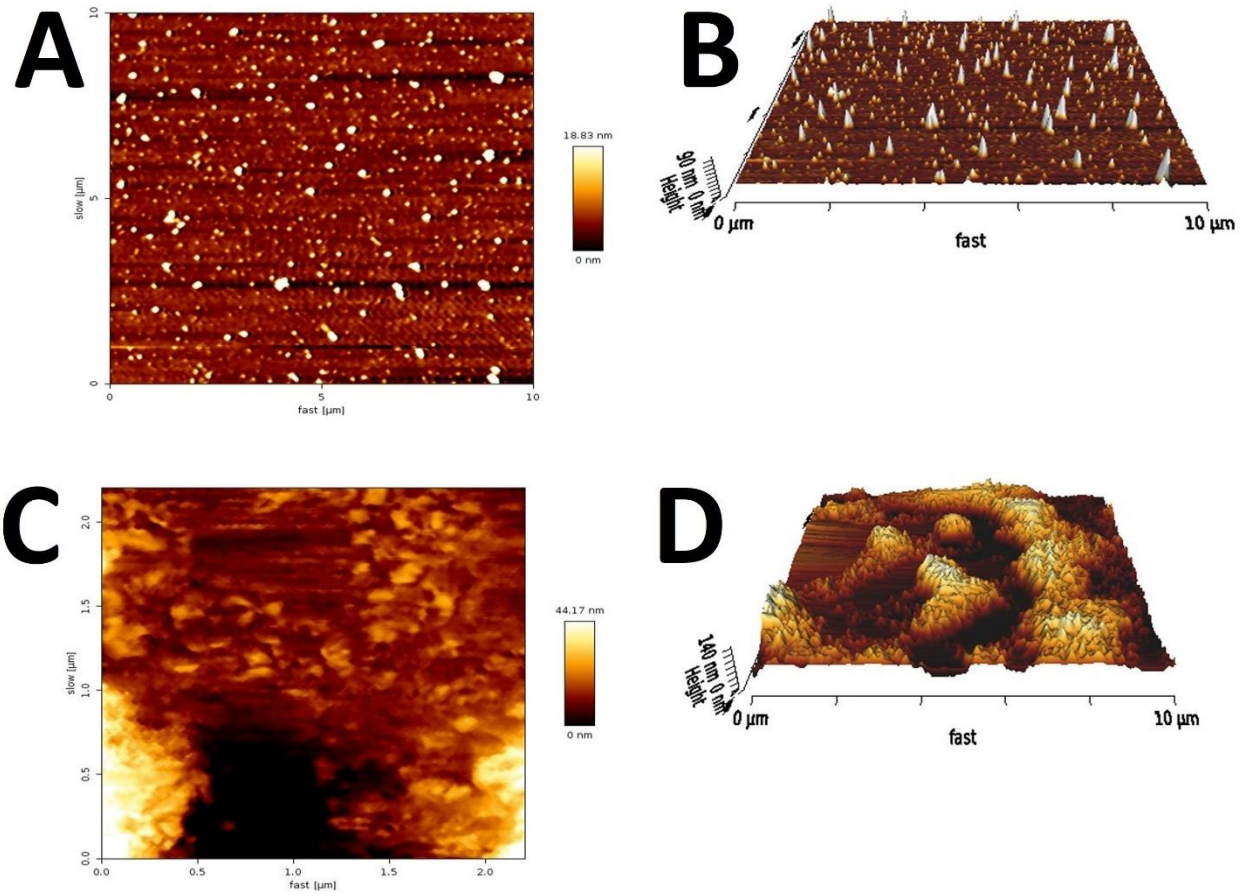

Figure 3. AFM topography of G2 dendrimer (**A**: 2D and **B**: 3D) and G2 dendrimer-BTX conjugate (D-BTX, **C**: 2D and **D**: 3D).

TEM analysis

TEM was used to examine the size and morphology of the G2 dendrimers and the D-BTX. High-resolution images are presented in Figure 4A and B. TEM images revealed that the unloaded G2 dendrimers were a small, well-defined, dense nanoparticle-like structure with an average diameter ranging from 7 to 10 nm. After conjugation with Botox, the D-BTX particles seemed larger and denser by electron microscopy, with most diameters being between 12 and 20 nm. Such morphological variation proved effective in the loading of the drug.

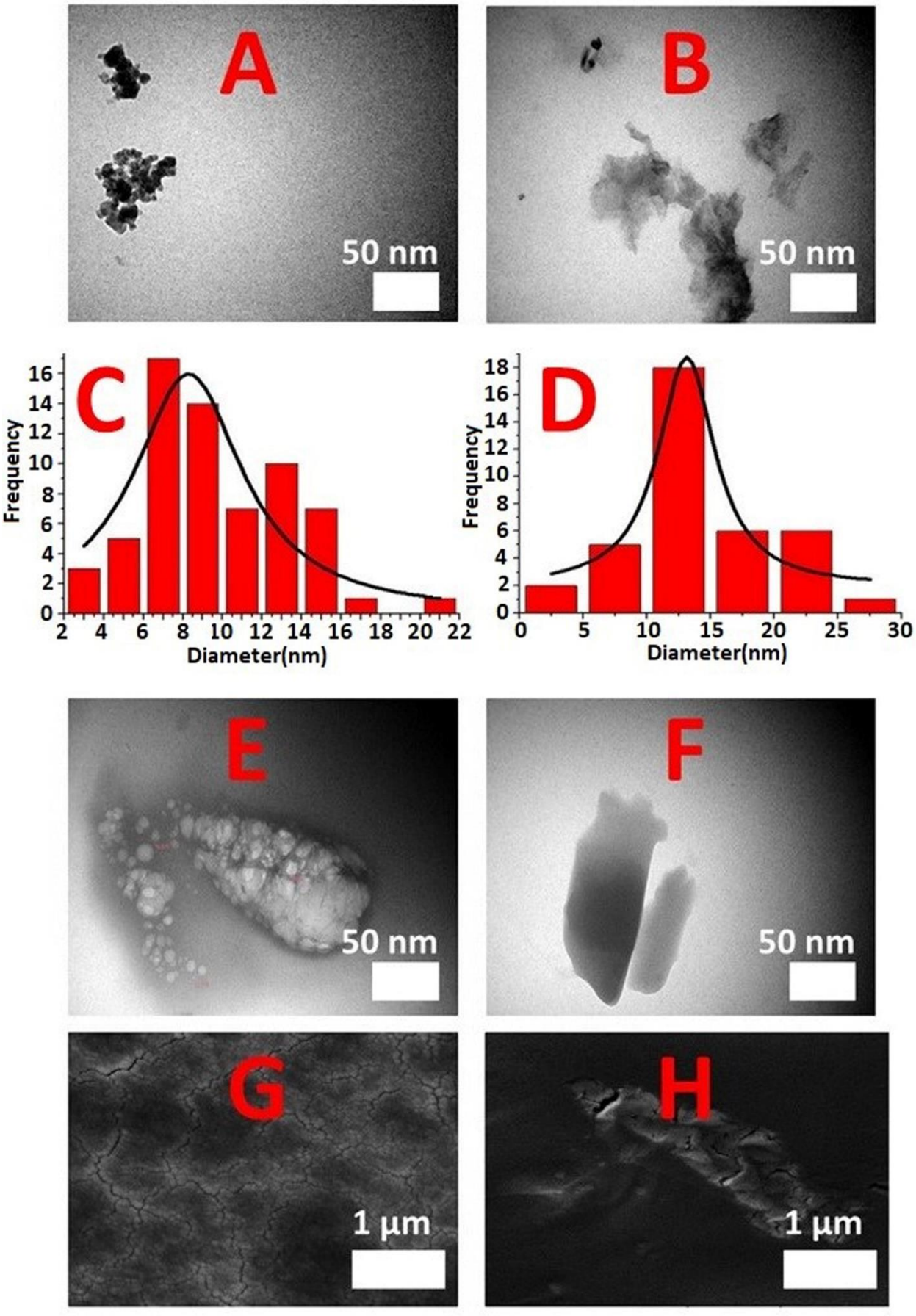
A
50 nm
B
50 nm
C
Frequency
Diameter(nm)
D
Frequency
Diameter(nm)
E
50 nm
F
50 nm
G
1 µm
H
1 µm

Figure 4. TEM micrographs of (**A**) unloaded G2 dendrimer and (**B**) G2 dendrimer-BTX conjugate (D-BTX) (Scale bar = 50 nm). Particle size distribution derived from TEM images for (**C**) unloaded G2 dendrimer and (**D**) D-BTX. TEM images of the D-BTX at (**E**) 3 months and (**F**) 6 months after synthesis. The images show well-dispersed, spherical nanoparticles with no visible aggregation or morphological changes, confirming the structural stability of the nanoconjugates over time. FE-SEM micrographs of (**G**) G2 dendrimer and (**H**) D-BTX.

In addition, particle size distribution analysis (Figure 4C and D) confirmed the increase in size observed following conjugation. The histogram showed that the most abundant G2 dendrimers were of the size 7–10 nm, whereas most D-BTX particles showed a size range of 12–20 nm. These findings also confirmed successful conjugation and structural modification of the dendrimeric carrier following contact with Botox.

FE-SEM analysis

Representative micrographs are shown in Figure 4G and H. The FE-SEM images revealed morphological differences between the unloaded G2 dendrimers and D-BTX conjugates. While the dendrimers were needle- or rod-shaped, more spherical and compact shapes were observed in the D-BTX compounds. In particular, the gel-like nature of the nano-dendrimers caused difficulties in sample preparation, which could lead to inhomogeneity of the surface structure. However, the uniformity of particle growth and the transformation from needle-like to spherical shapes were good evidence of the successful development of the nano-drug.

Colloidal stability of D-BTX nanoconjugates

Physicochemical stability of D-BTX was measured at the time of synthesis (month 0), and at three and six months post-synthesis. By DLS, no variation in particle size was detected over time. The mean hydrodynamic diameter was 160 ± 3.1 nm, 153 ± 2.5 nm, and 162 ± 2.8 nm at baseline, 3 months, and 6 months, respectively; therefore, there was a colloidal stability during storage (Table 2). TEM imaging at the 3rd and 6th months confirmed the preservation of spherical morphology and structural stability of the D-BTX nanoparticles without any detectable aggregation and deformation (Figure 4E and F). All these findings collectively establish that the D-BTX nanoconjugates preserve their size distribution, morphology, and overall structural stability for six months or more during storage, indicating their suitability for long-term biomedicine applications.

MTT cytotoxicity

The cytotoxicity of dendrimers, Botox, and D-BTX preparations against HFF2 cell lines was ascertained using the MTT assay. Statistical comparisons of differences among means of groups were made using Tukey's multiple comparisons test. The results are shown in Figure 5A. No significant difference in cell viability between PBS and dendrimers ($p > 0.9999$) was observed, indicating that dendrimers did not significantly affect cell viability compared to the control group. A comparison of BTX and D-BTX formulations at equivalent concentrations of 0.001, 0.01, and 0.1 ng/mL yielded the following results: An interesting decrease in cell viability was observed in the BTX 0.001 group compared to the D-BTX 0.001 group with a mean difference of -42.31 (95.00% CI of diff: -69.76 to -14.86; $p = 0.0013$), indicating the addition of dendrimers to BTX at this dose

reduced the cytotoxicity of BTX. However, there was no significant difference between BTX 0.01 and D-BTX 0.01 ($p = 0.0598$). Although there was decreased cell toxicity in the D-BTX 0.01 group, the result was not statistically significant, meaning that the addition of dendrimers to BTX at this level did not have a considerable effect on the cytotoxicity of BTX. Moreover, BTX 0.1 did not significantly differ from D-BTX 0.1 ($p = 0.6437$). The percentage of cell viability in both groups was equal, indicating that at this higher concentration, the effect of dendrimers on BTX cytotoxicity did not alter significantly.

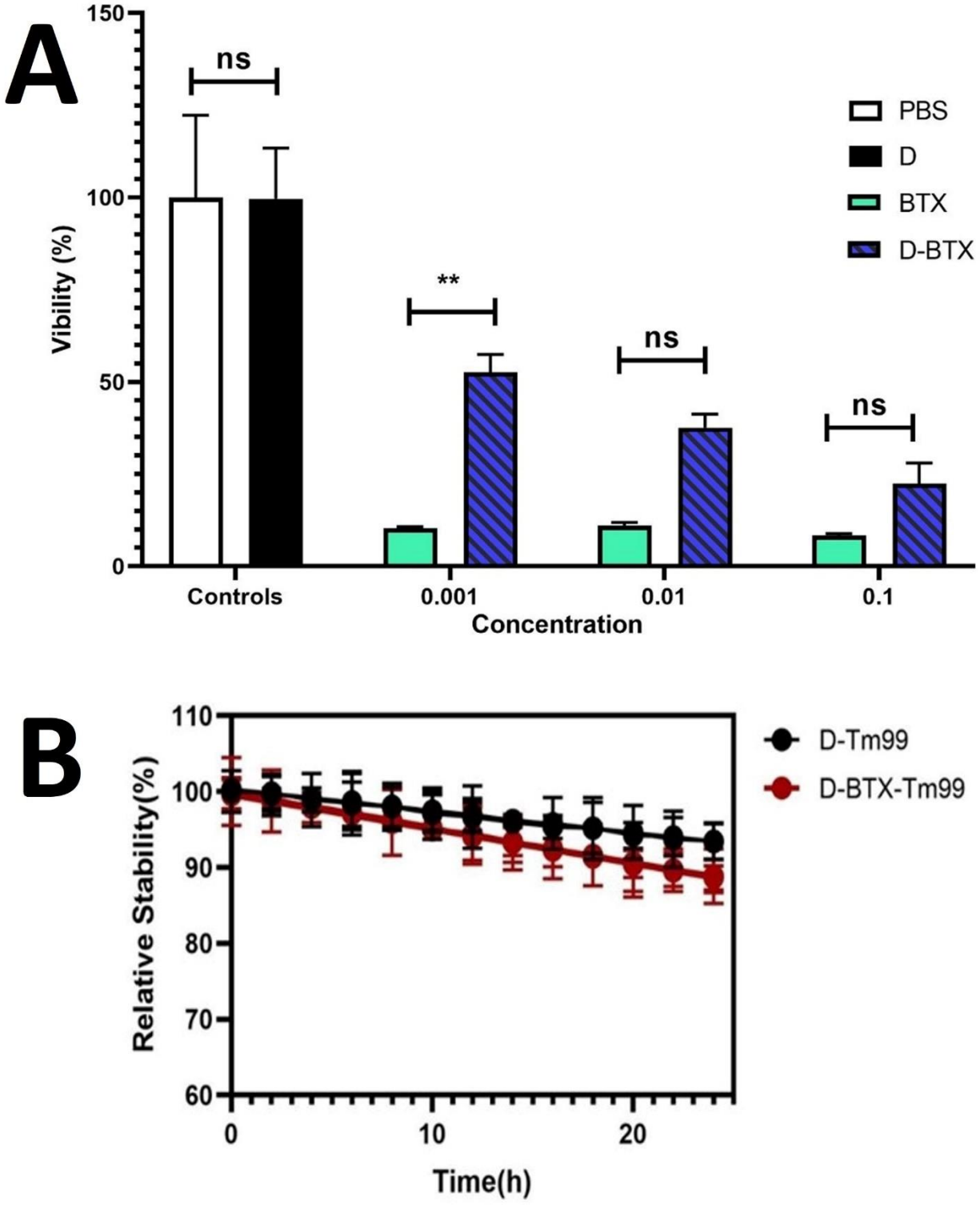

Figure 5. (A) Cytotoxic impacts of different concentrations (0.001, 0.01, and 0.1 ng/mL) of free dendrimers (D), free MASPORT®500 (BTX), and BTX-dendrimer conjugate (D-BTX) on the Human

foreskin fibroblast 2 (HFF2) cell lines were measured using the MTT assay. The data are reported as a percentage of the control (PBS-treated cells) considered as 100% viability, and all data are reported as means ± standard deviations of triplicate (**p < 0.01; ns, non-significance). (**B**) stability of ^{99m}Tc-labeled D-BTX nanoconjugates over time.

Radiochemical purity

The chromatogram (Figure S1 and S2) showed a very intense peak at Rf ~0.13 corresponding to the radiopharmaceutical complex (RPH1). A radiochemical impurity (IMP1) was present as a very minor peak at Rf ~0.04. The quantitative estimation gave radiochemical purity as 90.85%, and the impurity accounted for 9.15% of the total radioactivity. According to regulatory guidelines, i.e., those established by pharmacopoeias and the current Good Manufacturing Practices (cGMP) regulations, preclinical animal study samples of radiolabeled drugs need to exhibit radiochemical purity of ≥90%, while samples used in clinical (human) applications should be of ≥95% purity.[77, 78] Hence, the purity acquired was easily in line with the needs of this preclinical study.

Radiochemical stability

The RT-LC analysis demonstrated (Figure 5B) that both ^{99m}Tc-dendrimers and ^{99m}Tc-D-BTX nanoconjugates were in good radiochemical stability after 24-h incubation in PBS at 37 °C. Free ^{99m}Tc pertechnetate content was below 10% for both products at all investigated time points. Even 24 h after radiolabeling, over 85% of the ^{99m}Tc-radiolabeled D-BTX was intact, indicating that conjugation of Botox did not adversely affect radiochemical or physicochemical stability of the nanoparticle system ($p<0.05$). The findings attested to the qualification of both ^{99m}Tc-

dendrimers and ^{99m}Tc-D-BTX nanoconjugates for biomedical applications, such as diagnostic imaging and targeted drug delivery, where radiochemical stability is a concern.

Imaging study of ^{99m}Tc-formulations

To assess the *in vivo* kinetic stability of the produced nanoconjugates, SPECT imaging was performed at a series of time points (0 and 12 h post-injection) following intramuscular administration in healthy mice. Data on the *in vivo* distribution of all formulations are presented in Table 4 and Figure 6A. Among all tested formulations, D–BTX–^{99m}Tc had the highest muscle uptake (74.25 ± 12.67%), much higher than BTX–^{99m}Tc (36.39 ± 1.96%), free ^{99m}Tc (0.32 ± 0.38%), and dendrimer-only (D–^{99m}Tc, 0.00%). Statistical analysis using Tukey's multiple comparisons test revealed muscle uptake of D–BTX–^{99m}Tc to be significantly greater than in all other groups ($p < 0.005$). In addition, BTX–^{99m}Tc retained significantly higher concentrations in muscle than D–^{99m}Tc and free ^{99m}Tc ($p < 0.01$), confirming botulinum activity in muscle-targeting as well as showing increased retention provided by dendrimer conjugation. Other tissues showed a negligible uptake rate for both BTX-based formulations (D-BTX–^{99m}Tc and BTX–^{99m}Tc). Notably, free ^{99m}Tc showed rapid systemic spread with very high uptake by the gastrointestinal tract and stomach, consistent with the known biodistribution of pertechnetate.[79] Overall, the D–BTX–^{99m}Tc preparation displayed higher *in vivo* stability, muscle site-specific retention, and low off-target organ accumulation.

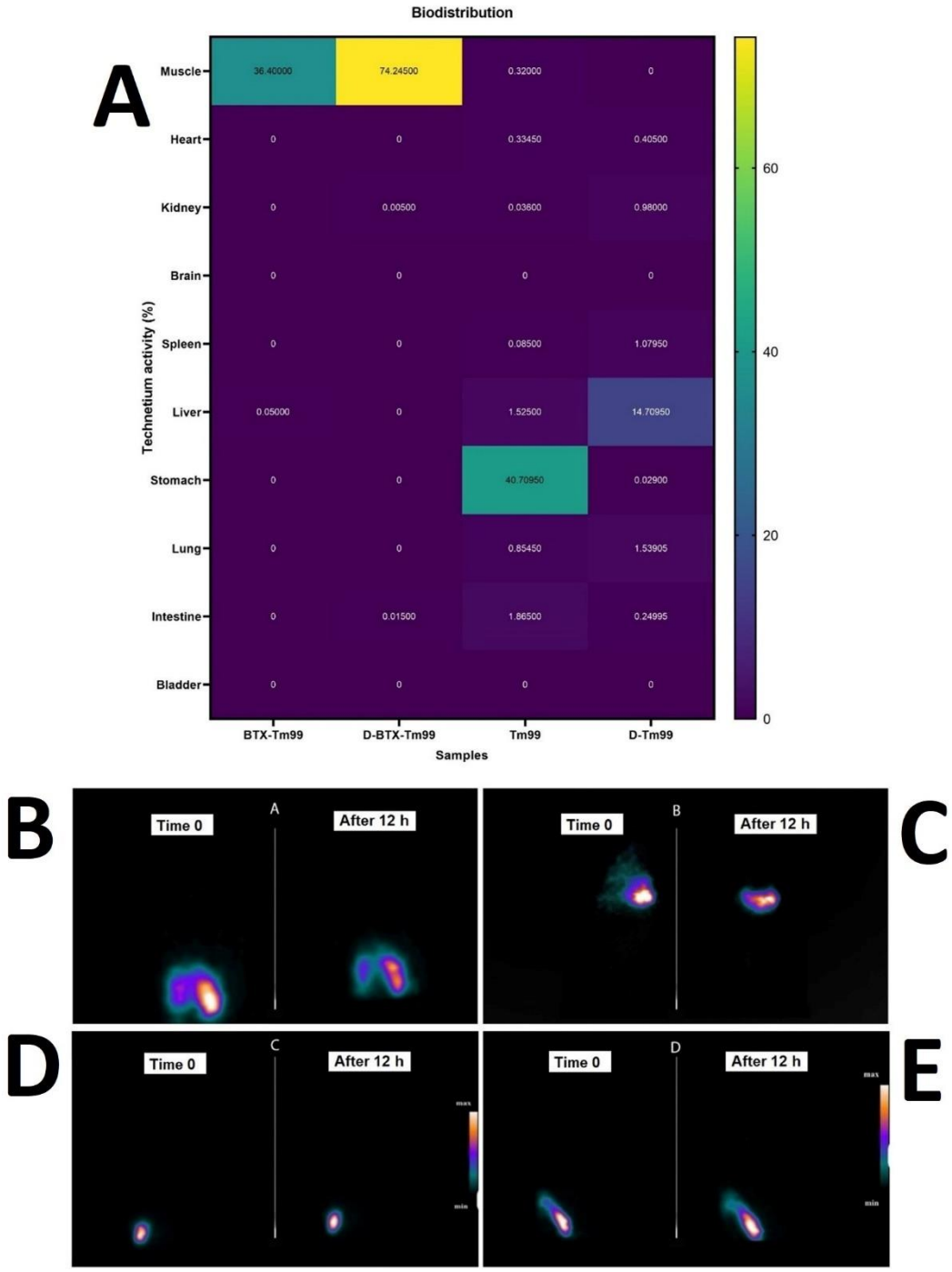

Samples	Area	Mean	Min	Max
free ^{99m}Tc (Time 0)	9234	90.753	12	254
free ^{99m}Tc (After 12 h)	7082	74.245	1	164
^{99m}Tc-dendrimers (Time 0)	4529	78.474	1	254
^{99m}Tc-dendrimers (After 12 h)	2229	97.507	5	251
^{99m}Tc-Labeled D-BTX (Time 0)	1152	84.747	6	230
^{99m}Tc-Labeled D-BTX (After 12 h)	1089	88.107	4	248

Figure 6. Visualization of the *in vivo* biodistribution analysis using a heatmap plot. Moreover, immediately and 12-h post-injection SPECT Imaging of the muscle tissue following the intramuscular injection of (**B**) free ^{99m}Tc, (**C**) ^{99m}Tc-dendrimer, (**D**) ^{99m}Tc-Labeled D-BTX nanoconjugate, and (**E**) ^{99m}Tc-BTX. The table also presents data derived from the quantification of muscle biodistribution images of technetium-labeled formulations using ImageJ software.

Evaluation of retention and localization of radiolabeled BTX formulations in muscle tissue

For comparison of localization and retention ability of various BTX-based preparations in the muscle tissue, the mean signal intensity and area of distribution were quantitatively analyzed through SPECT imaging and ImageJ software (Figure 6B to E). In the case of free ^{99m}Tc, mean intensity decreased sharply from 90.753 (Time 0) to 74.245 (12 h later), together with a drop in dispersion area from 9234 to 7082. This decrease was indicative of rapid diffusion of free ^{99m}Tc from the site of injection, confirming its low retention capability and high systemic leakage. On the other hand, ^{99m}Tc-dendrimers experienced a mean intensity increase from 78.474 to 97.507 between 0 and 12 h, and the area of distribution decreased significantly from 4529 to 2229. This is a reverse trend that showed that dendrimers effectively localized the radiotracer into a concentrated small volume of muscle tissue and enhanced retention but limited dispersion. Similarly, ^{99m}Tc-Labeled D-BTX nanoconjugates demonstrated high mean intensities, rising from 84.747 to 88.107, with a slight reduction in area from 1152 to 1089 after 12 h. The smaller change in both parameters indicates excellent stability, improved muscle localization, and reduced diffusion, hence making D-BTX highly suitable for long-term therapeutic effects at the target region. For ^{99m}Tc-BTX, an increase in mean intensity by a moderate degree of 85.269 to 90.201

and a modest growth in area from 2434 to 2784 were observed. Although this suggests good retention, the increase in area suggests a relatively greater diffusion than in D-BTX nanoconjugates.

Discussion

Herein, we successfully synthesized and characterized a dendrimer-botulinum Botox nanoconjugate derived from the second-generation ALGD as the carrier platform. Our results show greater physicochemical stability, biocompatibility, and muscle-targeted delivery of D-BTX-A compared to free Botox, circumventing long-standing issues with the conventional BOTOX®. *In vitro* and *in vivo* experiments, including cytotoxicity assays, radiochemical labeling, and biodistribution imaging, also supported the value of our nanoconjugate for biomedical applications in which precision and extended delivery of BOTOX® is required.

While outstanding advances in the synthesis of Botox-based nano-formulation have been documented, dendrimer-mediated delivery of Botox is a novel and rising topic of research. Despite this, dendrimers have already emerged with impressive promise as carriers of other therapeutic payloads due to their extremely branched, monodisperse, and surface-mutable architecture. More specifically, a fundamental property of ALGD dendrimers is that they are amphiphilic and anionic, making high drug loading possible with sustained release without resorting to stabilizing excipients.[42, 67, 70, 71, 80] Moreover, our rationale for employing ALGD dendrimers was further validated by prior research into PEG-based Botox delivery platforms. For example, Poly(lactic-co-glycolic acid) (PLGA)-PEG-PLGA copolymers, as well as other PEG-modified matrices, such as Poly(DL-lactide) (PDLLA)-PEG-PDLLA and P(L-co-CL)-PEG-P(L-co-CL),

have been shown to extend the *in vivo* neuromuscular blockade attributed to BTX-A for up to 30 days, compared to just a few days with free Botox. The duration of the paralysis was determined to be related to the composition of the polymer and excipients like PEG-400 Da.[49] These data further support the conclusion that PEG-based polymeric nanoparticles can extend the duration of BTX-A action and enhance its delivery to the target muscles, which is consistent with performance in our D-BTX nanoconjugate platform.

Although nanotechnology-based platforms, such as nanoemulsions, hydrogels, and polyelectrolyte complexes, have been found to be useful in prolonging the drug stability and activity of Botox (Table 5), our dendrimeric formulation has the additional benefit of structural accuracy and stability over a prolonged period. For example, nanoemulsion-based Botox delivery systems offered protection against environmental stresses, including pH, enzymatic hydrolysis, and heat, and maintained biological activity for a period of three weeks after application, with clinical effects of muscle relaxation and wrinkle smoothing up to 12 weeks.[10] Polymeric microparticles, including PLGA, have also been shown to prolong Botox activity. A particularly important finding was that a 1.5 U dose of PLGA-encapsulated Botox microparticles was effective for inducing neuromuscular paralysis in mouse models for up to 47 days—almost threefold the level of paralysis achieved with lower dosing of the free toxin. Yet the 1.5 U dose of the free Botox proved to be intolerable to the animals.[49] Similarly, flash nano-complexation and nano-precipitation of BTX-A toxoid and Botox with polyelectrolyte complexes (PEC) have enabled sustained, linear release profiles (e.g., 30–35% release over 30 days and ~75% over 98 days). This approach has also demonstrated increased functional longevity *in vivo*, significantly enhancing grip strength recovery and prolonging action duration compared to unencapsulated Botox.[53, 81]

New peptide-augmented nanocomplexes (e.g., cell-penetrating peptides (CPPs)-Botox) also highlight the potential of nano-architectures in controlling BTX release kinetics and its therapeutic efficacy. These platforms showed a slower onset with a more sustained neuromodulatory action—a beneficial profile for aesthetic or therapeutic neurological use.[27] In addition, electrochemically prepared BTX-nanocomplexes with colloidal silver nanoparticles are yet another novel strategy, significantly enhancing the Botox's shelf-life (up to 3–4 months refrigerated versus 1–2 weeks for standard BTX in saline). Clinical results also reflected a significant prolongation of the therapeutic duration of this formula—up to 11 months—among patients with periocular usage.[52] Hydrogel-based and thermo-sensitive Botox formulations, including carboxymethylcellulose (CMC)-BTX and TCGel®, also provide local biocompatibility with sustained release. Such safe delivery systems have shown efficacy in managing conditions such as painful bladder syndrome (PBS/IC), where clinical effects endured for 12 weeks after treatment.[46, 55, 82]

The remarkable originality of our research was the long-term colloidal stability of the D-BTX complex *in vitro*, sustained for six months without the use of cryoprotectants or surfactants. However, these *in vitro* findings need to be confirmed by functional potency tests, including FRET-based SNAP-25 endopeptidase assays, *in vivo* LD_{50} and paralysis assays in mouse models, and the Aoki scale scoring system.[10, 49, 52, 72] Of note, previous studies, such as those on CPP-Botox nanocomplexes, have reported that freeze-drying with excipients (e.g., trehalose and polysorbate 20) is necessary to maintain structural integrity. In their trials, SEM observation of resolubilized CPP-Botox particles verified that lyophilization did not alter particle shape or size. Additionally, the study identified PBS as the optimal solvent for yielding the smallest and most

uniform particles, likely due to the ionic strength and pH of the medium. These parameters were able to influence particle size and charge distribution, thereby affecting their stability and ability to form stable complexes.[27] In contrast, our D-BTX nanoconjugates showed their uniform shapes when stored for six months.

In addition, the D-BTX nanoconjugate stability test demonstrated greater long-term physicochemical stability compared to the commercial free Botox formulation (Masport; Table 1). Over a period of six months' storage at 4 °C, D-BTX exhibited a stable hydrodynamic diameter with only slight changes being observed (160 ± 3.1 nm when synthesized, 153 ± 2.5 nm after 3 months, and 162 ± 2.8 nm after 6 months), indicating very good colloidal stability. TEM imaging also verified the preservation of spherical morphology and absence of aggregation or structural deformation during storage. In comparison, the Masport brand, a lyophilized abobotulinum toxin A preparation stabilized in lactose and human albumin, has a reported shelf-life of only three months prior to reconstitution and limited post-reconstitution stability of just 8 h when kept under recommended refrigeration (2–8 °C).[21, 22] The marked disparity in long-term stability underscores the advantage of the dendrimer-based conjugation method employed in the D-BTX formulation. By providing increased durability against environmental stressors and minimization of protein denaturation or aggregation, D-BTX offers a robust alternative with prolonged storage capability, making it more suitable for biomedical applications where longer shelf-life and reproducible performance are paramount. This heightened stability not only avoids the native botulinum toxin's natural lability but also provides a practical means to avoid cold chain logistic problems and product wastage in the clinic.

From a safety standpoint, our dendrimer-based delivery system has some clear benefits over newer formulations of Botox containing surfactants and virus-derived excipients. For instance, Daxxify®, containing RTP004 and polysorbate 20, has been linked to adverse events (AEs) in as many as 20% of patients, while liquid Botox formulations such as Alluzience® have recorded even higher AEs in several studies.[83] Since there are limited long-term safety data available for polysorbate-containing products, our dendrimer-based strategy, excipient-free of such additives, can potentially be a safer and more pharmacologically controlled option. Such characteristics may translate into better patient outcomes and fewer risks of treatment-related adverse effects.

The physicochemical characterization conducted in our research confirmed the effective synthesis and formulation of the D-BTX complex. The calculated ~43% increase in hydrodynamic diameter after conjugation—from 111.6 ± 16.9 nm to 160.0 ± 3.1 nm—was in agreement with the literature on ALGD-based drug delivery systems, further confirming the effectiveness of our approach.[66-71] In addition, the reported zeta potential shift from –25.2 mV to +17.16 mV is a strong indication of successful electrostatic and covalent binding between the anionic dendrimer and cationic sites of BTX-A—a feature also reported in previous nanoconjugate works by Zadeh Mehrizi *et al*.[71, 80] Compared to other nanotechnology-based Botox delivery systems, some significant differences are apparent. Nanoemulsion systems, for example, through high-pressure microfluidization, exhibited a wide range of sizes (10–300 nm) and zeta potentials, which lacked the precise control that our dendrimer-based system offers.[10] Moreover, CPP-Botox nanocomplexes had a size range of 308 ± 15 nm to 221 ± 8 nm, also reflecting the greater uniformity and control of our dendrimeric system.[27]

Regarding biocompatibility, our research revealed that the low concentration of D-BTX (0.001 ng/mL) induced a considerable decrease in the cytotoxicity of free Botox. However, this effect was not seen at higher concentrations of 0.01 and 0.1 ng/mL. Compared to other earlier Botox delivery approaches, our approach has several evident advantages. For example, Shabani *et al*.[27] illustrated that their CPP-Botox nanocomplexes internalized efficiently into NIH-3T3, which was correlated with long-term increased toxicity due to improved cellular uptake.[27] Even though these approaches achieve the best therapeutic outcome, they are likely to deliver more off-target cytotoxicity as well. In contrast, our dendrimer-based approach was muscle-targeted and reduced nonspecific uptake, with a better safety-to-efficacy ratio. Moreover, our D-BTX formulation tended to reduce the inherent cytotoxicity of free Botox at 0.001 ng/mL. This can be attributed to the protective cover offered by the PEG-based dendrimer matrix.

One of the significant strengths of the current work is its detailed *in vivo* biodistribution study of the ^{99m}Tc-labeled D-BTX nanoconjugate. After intramuscular delivery, the construct was found to be highly specific for targeting muscle tissue with very minimal off-target organ accumulation. Such specificity is extremely beneficial for the treatment of localized neuromuscular diseases. Notably, such targeting specificity at this level has not been routinely demonstrated in other nanoformulated Botox systems.[27, 49, 53, 81] However, the current study had a few flaws, the major among them being the absence of longitudinal functional testing in dominant models of neuromuscular dysfunction.

Most importantly, by determining the quantification of retention and dispersion of radiolabeled BTX formulation in muscles, we established that the D-BTX nanoconjugates possess the most optimal profile with the highest retention (stable/increased mean intensity) and least

tissue dispersion (stable area). This increased BTX localization in muscles, which is highly essential for optimal BTX therapeutic efficacy and restricted off-target activity in adjacent tissues. Further, the ^{99m}Tc-radiolabeled nanoconjugate of D-BTX allows for real-time, noninvasive tracking of tissue-selective delivery with SPECT imaging. Radiochemical purity (≥90%) and structural integrity were retained following more than 24 h (>85% intact), and the construct proved to have imaging capability without sacrificing therapeutic activity. The inherent characteristics of the dendrimer carrier—high branching, internal cavity volume, and numerous surface functional groups—position it well as a platform for such dual-mode use. Prior research by Hashempour Alamdari et al. (2017) and Mirzaei et al. (2015) has established G2-ALGD conjugates as a suitable vehicle for combined imaging and therapy in biological systems, reinforcing the viability of this platform.[68, 69] In particular, their work demonstrated gadolinium-encapsulated G2 dendrimers conjugated with ligands to target tumors for tumor-specific MRI imaging and therapeutic application. Expanding upon these ideas, our D-BTX construct and ^{99m}Tc-radiolabeling strategy broadens this paradigm to neuromuscular disorders, which places dendrimer–botulinum formulations as next-generation precision nanomedicines.

Limitations and Future Perspectives

We completely understood that the next critical step was to test the biological activity and biostability of our Botox-dendrimer conjugates *in vivo*. However, due to the financial and resource constraints inherent to this project, we were unable to extend our work to *in vivo* functional potency assays at this stage. Therefore, we accept this as a limitation and explicitly state that our future research will focus on *in vivo* validation of the retained biological activity

and therapeutic efficacy of the G2-ALGD-Botox formulation. Indeed, the ultimate practical value of this system depends on a thorough *in vivo* validation.

Conclusion

In summary, we were able to synthesize and characterize a PEGylated dendrimer-Botox (D-BTX) nanoconjugate as a solution to the instability and uncontrolled diffusion of the native Botox formulation. Conjugation onto G2-ALGDs significantly enhanced the physicochemical stability of Botox by presenting increased particle size, altered surface charge, and stable amide bond formation. This preparation was of good cytocompatibility at low levels and had structural stability following six months of cold storage. Radiolabeling with high-purity technetium-99m was achieved with short-term stability, allowing effective imaging. SPECT analysis confirmed enhanced muscle localization and retention of D-BTX with minimal diffusion from the injection site. For enabling clinical translation successfully, broad-based studies should be conducted for assessing long-term functional performance, dosing regimen tailoring, and establishing safety in late-stage translational animal models.

References

1. Rempel L, Malik RN, Shackleton C, Calderón-Juárez M, Sachdeva R, Krassioukov AV, et al. From Toxin to Treatment: A Narrative Review on the Use of Botulinum Toxin for Autonomic Dysfunction. Toxins 2024;16(2):96. DOI: https://doi.org/10.3390/toxins16020096.
2. Rossetto O, Pirazzini M, Fabris F, Montecucco C. Botulinum neurotoxins: mechanism of action. Handb Exp Pharmacol 2021; 263:35-47. DOI: https://doi.org/10.1007/164_2020_355.
3. Kumar R and Singh BR. Botulinum Toxin: A Comprehensive Review of Its Molecular Architecture and Mechanistic Action.
Int J Mol Sci 2025;26(2):777. DOI: https://doi.org/10.3390/ijms26020777.
4. Onan D, Farham F and Martelletti P. Clinical conditions targeted by OnabotulinumtoxinA in different ways in medicine. Toxins 2024;16(7):309. DOI: https://doi.org/10.3390/toxins16070309.
5. Wong ZY, Damavandi P, Richards M, Danpanichkul P, Adegboye O, Faderani R, et al. Botulinum Toxin in Aesthetic Medicine: A Bibliometric Analysis of Research Trends and Methodological Quality of the Top 100 Cited Publications. Aesthet Surg J Open Forum 2025;8:7:ojae131. DOI: https://doi.org/10.1093/asjof/ojae131.
6. Kadir SD. Industrial Production and Therapeutic Application of Botulinum Neurotoxin: The Role of C. botulinum Type A. Pharm Nanotechnol 2024;12(2):99-07. DOI: http://dx.doi.org/10.2174/2211738511666230825150259.
7. Dong M and Stenmark P. The structure and classification of botulinum toxins. Handb Exp Pharmacol 2021;263:11-33. DOI: https://doi.org/10.1007/164_2019_342.
8. Brin MF, Nelson M, Ashourian N, Brideau-Andersen A, Maltman J. Update on non-interchangeability of botulinum neurotoxin products. Toxins 2024;16(6):266. DOI: https://doi.org/10.3390/toxins16060266.
9. Choudhury S, Baker MR, Chatterjee S, Kumar H. Botulinum toxin: an update on pharmacology and newer products in development. Toxins 2021;13(1):58. DOI: https://doi.org/10.3390/toxins13010058.
10. Edelson J and Nicolosi R. Botulinum nanoemulsions. Google Patents, 2022.
11. Antonucci F and Bozzi Y. Action of Botulinum Neurotoxin E Type in Experimental Epilepsies. Toxins 2023;15(9):550. DOI: https://doi.org/10.3390/toxins15090550.
12. Park MY and Ahn KY. Scientific review of the aesthetic uses of botulinum toxin type A. Arch Craniofac Surg 2021;22(1):1. DOI: https://doi.org/10.7181/acfs.2021.00003.
13. Avelar R. Botulinum Toxin Accessory Proteins: Are They Just an Accessory? Dermatol Surg 2014:69-01. DOI: https://doi.org/10.1097/dss.0000000000004284.
14. Lee CG, Oum JH, Ajay V, Gui X. Cell-based method for determining an activity of botulinum toxin. Google Patents, 2021.

15. Martínez-Carranza M, Škerlová J, Lee P-G, Zhang J, Krč A, Sirohiwal A, et al. Activity of botulinum neurotoxin X and its structure when shielded by a non-toxic non-hemagglutinin protein. Commun Chem 2024;7:179. DOI: https://doi.org/10.1038/s42004-024-01262-8.
16. Witmanowski H and Błochowiak K. The whole truth about botulinum toxin, a review. Postepy Dermatol Alergol 2019;37(6):853–61. DOI: https://doi.org/10.5114/ada.2019.82795.
17. Field M, Splevins A, Picaut P, Schans M, Langenberg J, Noort D, et al. AbobotulinumtoxinA (Dysport®), OnabotulinumtoxinA (Botox®), and IncobotulinumtoxinA (Xeomin®) Neurotoxin Content and Potential Implications for Duration of Response in Patients. Toxins (Basel) 2018;10(12):535. DOI: https://doi.org/10.3390/toxins10120535.
18. Dover JS. Introduction to the supplement: A review of abobotulinumtoxinA (Dysport). Aesthet Surg J Open Forum 2017;37(Suppl 1):S1–S3. DOI: https://doi.org/10.1093/asj/sjw281.
19. Coleman K. Botulinum Toxin in Facial Rejuvenation E-Book: Botulinum Toxin in Facial Rejuvenation E-Book. Elsevier Health Sciences, 2019.
20. Salame N, Eber AE and Dover J. DaxibotulinumtoxinA-lanm (Daxxify™): A Comprehensive Overview. Skin Therapy Lett 2023;28(4):1-3.
21. Hedayat K and Ehsani AH. A Phase III Clinical Study of the Efficacy and Safety of Botulinum Toxin Type A (MASPORT) with DYSPORT for the Treatment of Glabellar Lines. Aesthetic Plast Surg 2024;48(3):324-32. DOI: https://doi.org/10.1007/s00266-023-03766-5.
22. Ehsani A, Ehsani AR, Razavi Z, Koohian Mohammadabadi M, Ansari M, Aryanian Z, et al. Botulinum toxins, Masport® vs Dyston®: Comparison of efficacy, side effects and duration of effect. J Dermatol Cosmet 2024;15(2):83-91.
23. Tian R, Widel M and Imanian B. The light chain domain and especially the C-terminus of receptor-binding domain of the botulinum neurotoxin (BoNT) are the hotspots for amino acid variability and toxin type diversity. Genes 2022;13(10):1915. DOI: https://doi.org/10.3390/genes13101915.
24. Montal M. Botulinum neurotoxin: a marvel of protein design. Annu Rev Biochem 2010;79:591-17. DOI: https://doi.org/10.1146/annurev.biochem.051908.125345.
25. Buzzatto MV, Benegas Guerrero FC, Álvarez PA, Zizzias MP, Polo LM, Tomes CN. Expression, purification and application of a recombinant, membrane permeating version of the light chain of botulinum toxin B. Biosci Rep 2024;44(7):BSR20240117. DOI: https://doi.org/10.1042/bsr20240117.
26. Lalaurie CJ. Structural Studies of pH Effects on Botulinum Toxins A & E. 2023.
27. Ravari NS, Sheikhlou MG, Goodarzi N, Kharazian B, Amini M, Atyabi F, et al. Fabrication, characterization and evaluation of a new designed botulinum toxin-cell penetrating peptide nanoparticulate complex. Daru 2023;31(1):1-12. DOI: https://doi.org/10.1007/s40199-023-00462-2.

28. Nuwarda RF, Ramadhania ZM and Novianti MT. The Stability of Protein Therapeutics: A Significant Challenge in the Formulation of Biopharmaceuticals. Indones J Pharm Sci Technol 2024;6:1-14. DOI: http://dx.doi.org/10.24198/ijpst.v6i2.56009.
29. Lee KWA, Chan LKW, Lee AWK, Lee CH, Wan J, Yi KH. Immunogenicity of botulinum toxin type A in different clinical and cosmetic treatment, a literature review. Life 2024;14(10):1217. DOI: https://doi.org/10.3390/life14101217.
30. Ton JL, Patel HA, Bates RC, Ahmad WM. Process and system for obtaining botulinum neurotoxin. Google Patents, 2021.
31. Martin MU, Frevert J and Tay CM. Complexing protein-free botulinum neurotoxin A formulations: implications of excipients for immunogenicity. Toxins 2024;16(2):101. DOI: https://doi.org/10.3390/toxins16020101.
32. Thompson SA, Ruegg CL and Waugh JM. Albumin-free botulinum toxin formulations. Google Patents, 2022.
33. Crook JL, Jahromi AH and Konofaos P. Long-term effects of repeated botulinum toxin injection in cosmetic therapeutics. Ann Plast Surg 2022;88(3):345-52. DOI: https://doi.org/10.1097/sap.0000000000002994.
34. Solish N, Carruthers J, Kaufman J, Rubio RG, Gross TM, Gallagher CJ, et al. Overview of daxibotulinumtoxinA for injection: a novel formulation of botulinum toxin type A. Drugs 2021;81(18):2091-01. DOI: https://doi.org/10.1007/s40265-021-01631-w.
35. Kroumpouzos G, Kassir M, Gupta M, Patil A, Goldust M. Complications of Botulinum toxin A: An update review. J Cosmet Dermatol 2021; 20(6): 1585-90. DOI: https://doi.org/10.1111/jocd.14160.
36. Sethi N, Singh S, DeBoulle K, Rahman E. A review of complications due to the use of botulinum toxin A for cosmetic indications. Aesthetic Plast Surg 2021;45(3):1210-20. DOI: https://doi.org/10.1007/s00266-020-01983-w.
37. Ebrahimi B, Jamzad S, Naseh Z, Moezzi I, Kargar Jahromi H, Naseh M. The efficacy of various interventions as good strategies to reduce pain in botulinum neurotoxin A for wrinkles. A systematic review of the randomized controlled trials (RCTs). J Cosmet Laser Ther 2024;26(1-4):69-76. DOI: https://doi.org/10.1080/14764172.2024.2374812.
38. Wee SY and Park ES. Immunogenicity of botulinum toxin. Arch Plast Surg 2022;49(1):12-18. DOI: https://doi.org/10.5999/aps.2021.00766.
39. Carr WW, Jain N and Sublett JW. Immunogenicity of botulinum toxin formulations: potential therapeutic implications. Adv Ther 2021;38(10):5046-64. DOI: https://doi.org/10.1007/s12325-021-01882-9.
40. Rahman E and Carruthers JDA. Immunogenicity of botulinum toxin A: insights. Dermatol Surg 2024;50(9S):S117-26. DOI: https://doi.org/10.1097/DSS.0000000000004293.
41. Rashied R and Gold MH. Innovation in Botulinum Toxins. Dermatol Clin 2025;43(1):55-66. DOI: https://doi.org/10.1016/j.det.2024.08.004.

42. Zadeh Mehrizi T. Assessment of the effect of polymeric nanoparticles on storage and stability of blood products (red blood cells, plasma, and platelet). Polym Bull (Berl) 2023;80(3):2263-98. DOI: https://doi.org/10.1007/s00289-022-04147-9.
43. Mehrizi TZ. Impact of metallic, quantum dots and carbon-based nanoparticles on quality and storage of albumin products for clinical use. Nano 2021;16(14):2130013. DOI: https://doi.org/10.1142/S1793292021300139.
44. Mehrizi TZ, Rezayat SM and Shahmabadi HE. Latest Findings on the Effects of Gold Nanoparticles on the Storage Quality of Blood Products (2011-2022)-A Narrative Review. Curr Drug Deliv 2025;22(5):537-51. DOI: 10.2174/0115672018316266240909075316.
45. Yusuf A, Almotairy ARZ, Henidi H, Alshehri OY, Aldughaim MS. Nanoparticles as drug delivery systems: a review of the implication of nanoparticles' physicochemical properties on responses in biological systems. Polymers 2023;15(7):1596. DOI: https://doi.org/10.3390/polym15071596.
46. An JM, Shahriar SMS, Lee DY, Hwang SR, Lee YK. Pore size-dependent stereoscopic hydrogels enhance the therapeutic efficiency of botulinum toxin for the treatment of nerve-related diseases. ACS Appl Mater Interfaces 2022;14:19139-53. DOI: https://doi.org/10.1021/acsami.2c01738.
47. Mehrizi TZ, Ardestani MS and Kafiabad SA. A review study of the influences of dendrimer nanoparticles on stored platelet in order to treat patients (2001-2020). Curr Nanosci 2022;18(3):304-18. DOI: https://doi.org/10.2174/1566524021666210708154736.
48. Mehrizi TZ and Ardestani MS. The introduction of dendrimers as a new approach to improve the performance and quality of various blood products (platelets, plasma and erythrocytes): a 2010-2022 review study. Curr Nanosci 2023;19(1):103-22. DOI: https://doi.org/10.2174/1573413718666220728141511.
49. Park K, Yun Y, Skidmore SM, Lee BK, Garner JS. Biodegradable polymer formulations for extended efficacy of botulinum toxin. Google Patents, 2023.
50. Malek-Khatabi A, Rad-Malekshahi M, Shafiei M, Sharifi F, Motasadizadeh H, Ebrahiminejad V, et al. Botulinum toxin A dissolving microneedles for hyperhidrosis treatment: design, formulation and in vivo evaluation. Biomater Sci 2023;11(24):7784-04. DOI: https://doi.org/10.1039/d3bm01301d.
51. Bhoopalam M, Qiu C, Harris TGW, Tuffaha S, Mao HQ, Reddy SK. 14. A Tunable Nanoparticle-based Botulinum Toxin Formulation for Extended Duration of Therapeutic Effect. Plast Reconstr Surg Glob Open 2023;11(5 Suppl):9-10. DOI: https://doi.org/10.1097/01.GOX.0000937652.43692.e5.
52. Moeller KW and Willoughby AJM. Botulinum toxin and colloidal silver particles. Google Patents, 2022.
53. Harris T, Qiu C, Colakoglu S, Tuffaha S, Mao HQ, Reddy SK. Extended Local Release of Neuromodulators from a Novel Nanoparticle System for Chronic Migraine and Facial Aesthetics.

Plast Reconstr Surg Glob Open 2021;9(10 Suppl):134-35. DOI: https://doi.org/10.1097/01.GOX.0000799792.25384.56.
54. Wang R-J, Wang Y, Wu J-F, Si T-T. Clinical effect of botulinum toxin type A combined with autologous fat grafting in patients with nasolabial fold depression. World J Clin Cases 2024;12(22):4973-82. DOI: https://doi.org/10.12998/wjcc.v12.i22.4973.
55. Stav K, Vinshtok Y, Jeshurun M, Ivgy-May N, Gerassi T, Zisman A. PD20-03 pilot study evaluating safety and feasibility of intravesical instillation of botulinum toxin in hydrogel-based slow release delivery system in PBS/IC patients. Urology 2015;193:e398. DOI: https://doi.org/10.1016/j.juro.2015.02.674.
56. Liu Q and Liao L. Nano-BTA: a new strategy for Intravesical delivery of botulinum toxin a. Int Neurourol J 2022;26(2):92-01. DOI: https://doi.org/10.5213/inj.2142124.062.
57. Assuncao DPSF, Farago PV, Grassiol S, Justus B. Development, characterization and assessment of botulinum toxin type A incorporated in nanocarriers. Afr J Pharm Pharmacol 2016;10(43):926-35. DOI: https://doi.org/10.5897/AJPP2016.4636.
58. Alavi SE, Shahmabadi HE, Sharma LA, Sharma A. Nanoparticle-based drug delivery systems for non-surgical periodontal therapy: innovations and clinical applications. 3 Biotech 2025;15:269. 20250725. DOI: https://doi.org/10.1007/s13205-025-04443-x.
59. Alavi SE, Malik L, Matti R, Al-Najafi F, Shahmabadi HE, Sharma LA. Bioresponsive nanotechnology in pediatric dental drug delivery.
J Drug Deliv Sci Technol 2024;93:105436. DOI: https://doi.org/10.1016/j.jddst.2024.105436.
60. Alharthi S, Alrashidi AA, Almawash S, Shahmabadi HE, Alavi SE. Targeted antibacterial and anticancer therapeutics: PEGylated liposomal delivery of turmeric and cinnamon extracts-in vitro and in vivo efficacy. Drug Dev Ind Pharm 2025;51(3):231-43. DOI: https://doi.org/10.1080/03639045.2025.2463395.
61. Alharthi S, Alrashidi AA, Ziora Z, Shahmabadi HE, Alavi SE. Innovative PEGylated chitosan nanocarriers for co-delivery of doxorubicin and CpG in breast cancer therapy: Preparation, characterization, and immunotherapeutic potential. Med Oncol 2025;42(5):176. DOI: https://doi.org/10.1007/s12032-025-02714-4.
62. Almutairy B, Alharthi S, Shahmabadi HE, Alavi SE. Use of nanoemulsion for co-delivery of silibinin and cabazitaxel for prostate cancer treatment. Drug Dev Ind Pharm 2025;51(11):1591-06. DOI: https://doi.org/10.1080/03639045.2025.2552392.
63. Almutairy B, Alharthi S, Shahmabadi HE, Alavi SE. Optimized solid lipid nanoparticles for co-delivery of gentamicin and doxycycline: a novel approach to combat intracellular brucella abortus infections. World J Microbiol Biotechnol 2025;41(7):232. DOI: https://doi.org/10.1007/s11274-025-04427-2.
64. Almutairy B, Alharthi S, Shahmabadi HE, Alavi SE. Using nanostructured lipid carrier for the co-delivery of rifampicin and pentamidine for the treatment of cutaneous leishmaniasis. J Drug Deliv Sci Technol 2025;113:107306. DOI: https://doi.org/10.1016/j.jddst.2025.107306.

65. Alyami H, Alharthi S, Alqahtani AJ, Shahmabadi HE, Alavi SE. Enhanced antitumor efficacy of nanostructured lipid carrier co-loaded with docetaxel and 5-fluorouracil for targeted gastric cancer therapy. Med Oncol 2025;42(2):53. DOI: https://doi.org/10.1007/s12032-025-02603-w.
66. Alavidjeh MS, Haririan I, Khorramizadeh MR, Ghane ZZ, Ardestani MS, Namazi H. Anionic linear-globular dendrimers: biocompatible hybrid materials with potential uses in nanomedicine. J Mater Sci Mater Med 2010;21(4):1121-33. DOI: https://doi.org/10.1007/s10856-009-3978-8.
67. Haririan I, Alavidjeh MS, Khorramizadeh MR, Ghane ZZ, Ardestani MS, Namazi H. Anionic linear-globular dendrimer-cis-platinum (II) conjugates promote cytotoxicity in vitro against different cancer cell lines. Int J Nanomedicine 2010;5:63-75. DOI: https://doi.org/10.2147/ijn.s8595.
68. Mirzaei M, Mehravi B, Ardestani MS, Ziaee SAM. In Vitro Evaluation of Gd 3+-Anionic Linear Globular Dendrimer-Monoclonal Antibody: Potential Magnetic Resonance Imaging Contrast Agents for Prostate Cancer Cell Imaging. Mol Imaging Biol 2015;17(6):770-76. DOI: https://doi.org/10.1007/s11307-015-0841-9.
69. Hashempour Alamdari N, Alaei-Beirami M, Sadat Shandiz SA, Hejazinia H, Rasouli R, Saffari M, et al. Gd3+-asparagine-anionic linear globular dendrimer second-generation G2 complexes: novel nanobiohybrid theranostics. Contrast Media Mol Imaging 2017;2017:3625729. DOI: https://doi.org/10.1155/2017/3625729.
70. Mehrizi TZ, Ardestani MS, Khamesipour A, Hoseini MHM, Mosaffa N, Anissian A, et al. Reduction toxicity of Amphotericin B through loading into a novel nanoformulation of anionic linear globular dendrimer for improve treatment of leishmania major. J Mater Sci Mater Med 2018;29(8):1-14. DOI: https://doi.org/10.1007/s10856-018-6122-9.
71. Mehrizi TZ, Mosaffa N, Khamesipour A, Hoseini MHM, Shahmabadi HE, Ardestani MS, et al. A Novel Nanoformulation for Reducing the Toxicity and Increasing the Efficacy of Betulinic Acid Using Anionic Linear Globular Dendrimer. J Nanostruct 2021;11(1):143-52. DOI: https://doi.org/10.22052/JNS.2021.01.016.
72. Araco A and Francesco A. Prospective randomized clinical study of a new topical formulation for face wrinkle reduction and dermal regeneration. J Cosmet Dermatol 2021;20(9):2832-40. DOI: https://doi.org/10.1111/jocd.13937.
73. Boschi A, Uccelli L and Martini P. A picture of modern Tc-99m radiopharmaceuticals: Production, chemistry, and applications in molecular imaging. Appl. Sci. 2019;9(12):2526. DOI: https://doi.org/10.3390/app9122526.
74. Mushtaq S, Bibi A, Park JE, Jeon J. Recent progress in technetium-99m-labeled nanoparticles for molecular imaging and cancer therapy. Nanomaterials 2021;11(11):3022. DOI: https://doi.org/10.3390/nano11113022.
75. Najdian A, Amanlou M, Beiki D, Bitarafan-Rajabi A, Mirzaei M, Ardestani MS. Amino-modified-silica-coated gadolinium-copper nanoclusters, conjugated to AS1411 aptamer and

radiolabeled with technetium-99 m as a novel multimodal imaging agent. Bioorg Chem 2022;125(5):105827. DOI: https://doi.org/10.1016/j.bioorg.2022.105827.
76. Zia A, Aghdam HR, Saffari M, Farzaneh J, Hamedani MP, Ebrahimi SES, et al. Novel chitosan-quinic acid nanoparticles labeled with m 99 technetium for breast cancer imaging. Nanomed J 2022;9(3):231-40. DOI: https://doi.org/10.22038/nmj.2022.64517.1673.
77. Ballinger J, Bruchertseifer F, Dollé F, Fukumori N, Jalilian A, Krasikova R, et al. Quality Control in the Production of Radiopharmaceuticals. International Atomic Energy Agency, 2018. ISBN 978-92-0-107918-3
78. Radioisotopes I and Series R. Guidance for preclinical studies with radiopharmaceuticals. International Atomic Energy Agency: Vienna, Austria 2021;8. ISSN 2077-6462.
79. Zuckier LS, Dohan O, Li Y, Chang CJ, Carrasco N, Dadachova E. Kinetics of perrhenate uptake and comparative biodistribution of perrhenate, pertechnetate, and iodide by NaI symporter–expressing tissues in vivo. J Nucl Med 2004;45(3):500-07.
80. Mehrizi TZ, Khamesipour A, Ardestani MS, Hoseini MHM , Mosaffa N, Ramezani A. Comparative analysis between four model nanoformulations of amphotericin B-chitosan, amphotericin B-dendrimer, betulinic acid-chitosan and betulinic acid-dendrimer for treatment of Leishmania major: real-time PCR assay plus. Int J Nanomedicine 2019;2019(14):7593-07. DOI: https://doi.org/10.2147/IJN.S220410.
81. Harris TGW, Qiu C, Colakoglu S, Tuffaha S, Mao HQ, Reddy S. 46. Nanomaterial-based Neuromodulators for Extended Duration of Therapeutic Effect. Plast Reconstr Surg Glob Open 2022;10:31. DOI: http://doi.10.1097/01.GOX.0000842512.01197.ca.
82. Rappaport YH, Zisman A, Jeshurun-Gutshtat M, Gerassi T, Hakim G, Vinshtok Y, et al. Safety and feasibility of intravesical instillation of botulinum toxin-A in hydrogel-based slow-release delivery system in patients with interstitial cystitis-bladder pain syndrome: a pilot study. Urology 2018;114:60-65. DOI: https://doi.org/10.1016/j.urology.2017.12.028.
83. Sattler S, Gollomp S and Curry A. A Narrative Literature Review of the Established Safety of Human Serum Albumin Use as a Stabilizer in Aesthetic Botulinum Toxin Formulations Compared to Alternatives. Toxins 2023;15(10):619. DOI: https://doi.org/10.3390/toxins15100619.

Table 1. Comparison of different botox brands.

Generic name	**Abobotulinum toxin A**	**Abobotulinum toxin A**	**Daxxibotulinum toxin A**	**Onabotulinum toxin A**	**Abobotulinum toxin A**	**Incobotulinum toxin A**
Brand name	Masport	Dyston	Daxxify	Botox	Dysport	Xeomin
Manufacturer	Masoon Darou	Danesh bonyan imen vaccine alborz	Revance therapeutics	Allergan pharmaceuticals	Ipsen biopharm	Merz pharma
Registration year	2012	2017	2022	1991	2009	2010
Country of origin	Iran	Iran	USA	USA	UK	Germany
Packaging (U/vial)	500	300	500	100	500	100

Composition	Human Albumin; Lactose	Hemagglutinin & Non-hemagglutinin proteins; Human albumin; Lactose	RTP 004 Peptide; Polysorbate-20	Hemagglutinin & Non-Hemagglutinin proteins; Albumin 500 µg; Sucrose; Sodium chloride	Hemagglutinin & Non-Hemagglutinin proteins; Albumin 125 µg; Lactose	Albumin 1 mg; Sucrose
Molecular weight (kDa)	900	900-300	150	900	900-500	150
Preparation form	Lyophilized	Lyophilized	Lyophilized	Vacuum dried	Lyophilized	Lyophilized
Storage temperature	2-8 °C	2-8 °C	Room temperature	2-8 °C	2-8 °C	Room temperature
Shelf-life after reconstitution	8 h	8 h	72 h	36 h	24 h	36 h

Stability	3 months	3 months	6 months	3-4 months	4 months	3 months

Table 2. Physicochemical characteristics of free dendrimers and D-BTX conjugates.

Formulation	DLS					
	Mean diameter (nm)			Zeta potential (mV)		
	Baseline	After three months	After six months	Baseline	After three months	After six months
D	111.6 ± 16.9	-	-	–25.2 ± 1.63	-	-
D-BTX	160.0 ± 3.1	153 ± 2.5	162 ± 2.8	+17.16 ± 1.24	+2.42 ± 1.92	+3.86 ± 1.27

Table 3. Key FTIR absorption bands observed for dendrimer, botulinum toxin, and D-BTX conjugates.

Sample	Functional group	Frequency (cm^{-1})
Botox	N–H and O–H stretching	2900–3500
	Carbonyl (C=O) stretching	1000–1300
Citric Acid	C=O (carboxyl)	1600–1700
	O–H stretching	~3400
PEG-citric Dendrimer	N–H and O–H stretching	~3500
	Dendrimer carbonyl (C=O)	~1700
D-botox	C=O stretching (amide I)	1649

23 **Table 4.** Biodistribution analysis of ^{99m}Tc-labeled formulations.

Formula	**Organ**	**Active tissue (µCi)**	**Tissue weight (g)**	**% Activity**	**Total active tissue (µCi)**
BTX-^{99m}Tc	Muscle	597.9 ± 19.94	0.9785 ± 0.15	36.393 ± 1.96	1696.5 ± 188.79
	Heart	0.00	0.2805 ± 0.044	0.00	—
	Kidney	0.00	0.5515 ± 0.0106	0.00	—
	Brain	0.00	0.5795 ± 0.0035	0.00	—
	Spleen	0.00	0.383 ± 0.0919	0.00	—
	Liver	4.12	2.6805 ± 0.426	0.053 ± 0.035	—
	Stomach	0.05	1.0575 ± 0.306	0.00	—
	Lung	0.00	0.4155 ± 0.016	0.00	—
	Intestine	0.00	4.5865 ± 0.0346	0.00	—
	Bladder	0.00	0.5445 ± 0.622	0.00	—
D-BTX-^{99m}Tc	Muscle	1443.75 ± 930.90	1.011 ± 0.4341	74.245 ± 12.665	1823.5 ± 16.26
	Heart	0.00	110.578 ± 156.15	0.00%	—

	Kidney	0.055 ± 0.077	0.4675 ± 0.0148	0.005 ± 0.0077	—
	Brain	0.00	0.5385 ± 0.078	0.00%	—
	Spleen	0.00	0.225 ± 0.0212	0.00%	—
	Liver	0.01 ± 0.14	1.7705 ± 0.1435	0.0033 ±0.005	—
	Stomach	0.00	0.7715 ± 0.54	0.00%	—
	Lung	0.00	0.2705 ± 0.024	0.00%	—
	Intestine	0.875 ± 1.19	3.4435 ± 0.590	0.015 ± 0.015	—
	Bladder	0.00	0.3505 ± 0.30	0.00%	—
^{99m}Tc	Muscle	1.24	1.085	0.32 ± 0.3	2091.00 ± 25.3
	Heart	1.61	0.249	0.3345 ± 0.034	—
	Kidney	0.40	0.559	0.036 ± 0.008	—
	Brain	0.00	0.582	0.00%	—
	Spleen	0.81	0.448	0.085 ± 0.007	—
	Liver	87.83	2.982	1.525 ± 0.1626	—

	Stomach	664.70	0.841	40.70 ± 4.1146	—
	Lung	7.08	0.427	0.8545 ± 0.0912	—
	Intestine	164.60	4.562	1.865 ± 0.1909	—
	Bladder	—	—	—	—
D-^{99m}Tc	Muscle	0.00	0.602	0.00%	1949.00
	Heart	0.46	0.629	0.0405 ± 0.0007	—
	Kidney	17.65	0.918	0.98 ± 0.01414	—
	Brain	0.00	0.425	0.00	—
	Spleen	12.08	0.576	1.0795 ±0.0007	—
	Liver	929.10	3.240	14.7095 ± 0.0007	—
	Stomach	0.65	1.105	0.029 ± 0.0001	—
	Lung	22.22	0.575	1.53905 ± 0.623	—
	Intestine	25.20	5.119	0.24995 ± 0.0001	—
	Bladder	—	—	—	—

24

25

Table 5. Summary of intramuscularly injected BTX-A nanoformulations with enhanced storage stability or extended duration of action.

Ref.	Nano-botox formulation	Synthesis method	Characterizations	Drug release	Administration route	Stability & *In vitro* findings	Toxin / Brand (serotype)
[10]	Banoemulsions	High-pressure microfluidization	10–300 nm; Zeta potential (mV): −50 to +50 OR −25 to +25 OR −10 to +10	Not mentioned	IM; transdermal	High resistance to environmental stressors	BOTOX®, DYSPORT®, Wako Chemicals (A, B, C1, C2, D, F, G)
[27]	CPP-Nanocomplexes	PEC	221–308 nm	Delayed onset, prolonged effect	IM	Stable post-lyophilization	Masport® (A)

[49]	PLGA-based microparticles	Emulsion/microfabrication	<100 µm	PLGA with lactide-to-glycolide (L: G) ration 75:25 (98%); PLGA with L: G 85:15 (94%)	IM	Fluorescence resonance energy transfer (FRET) assay confirmed bioactivity	List biolabs (A)
[53, 81]	PEC nanoparticles	Flash nano-complexation/nano-precipitation	Not mentioned	30%-35% in 30 days, ~75% in 98 days)	IM	Stable at 25°C for 70 days	A, toxoid